Supporting Information

Calix[*n*]triazolium based turn-on fluorescent sensing ensemble for selective adenosine monophosphate (AMP) detection

Jihee Cho,[a,†] Jinwoo Shin,[b,†] Minjung Kang,[b,†] Peter Verwilst,[c] Changhyun Lim,[a] Hanbin Yoo,[a] Jeung Gon Kim,[d] Xingcai Zhang,[e,f] Chang Seop Hong,[b,*] Jong Seung Kim[b,*] and Sanghee Kim[a,*]

[a] College of Pharmacy, Seoul National University, 1 Gwanak-ro, Gwanak-gu, Seoul 08826, Korea

[b] Department of Chemistry, Korea University, Seoul 02841, Korea

[c] KU Leuven, Rega Institute for Medical Research, Medicinal Chemistry, Leuven 3000, Belgium

[d] Department of Chemistry and Research Institute of Physics and Chemistry, Jeonbuk National University, Jeonju 54896, Korea

[e] John A. Paulson School of Engineering and Applied Sciences, Harvard University, Cambridge, Massachusetts 02138, U.S.A.

[f] School of Engineering, Massachusetts Institute of Technology, Cambridge, Massachusetts 02139, U.S.A.

[†] These authors contributed equally.

* Corresponding author. E-mail: cshong@korea.ac.kr (C. S. H.), jongskim@korea.ac.kr (J. S. K.), pennkim@snu.ac.kr (S. K.)

Author Contributions

J. Cho performed all experimental work and wrote the manuscript and supplementary information. J. Shin performed the DFT calculations. M. Kang and C. S. Hong solved and refined the X-ray single-crystal structures. P. Verwilst performed the DFT calculations and corrected the manuscript. C. Lim and H. Yoo helped to synthesize the compounds. J. G. Kim and X. Zhang provided helpful discussions related to the ball-milling process. J. S. Kim supervised the project. S. Kim designed the project, provided supervision, and wrote the manuscript. All authors discussed the results and commented on the manuscript.

Contents

1. Synthesis

General methods. All of the chemicals used were reagent grade and were used as purchased. Reactions in solvents were performed under an inert atmosphere of dry nitrogen, using distilled dry solvents. The reaction progress was monitored by thin layer chromatography (TLC) analysis using silica gel 60 F-254 TLC plates. The compound spots were visualized using UV light. Melting points were measured using a Buchi B-540 melting point apparatus without correction. ^{1}H and ^{13}C NMR spectra were recorded on JEOL JNM-ECZ400S/L1 (400 MHz), Bruker Avance-500 (500 MHz) or Jeol JNM-ECA-600 (600 MHz) spectrometer at 278K. Chemical shifts are reported in ppm (δ) units relative to the undeuterated solvent as a reference peak (DMSO–d_6: 2.50 ppm/^{1}H NMR, 39.52 ppm/^{13}C NMR). The following abbreviations are used to represent NMR peak multiplicities: s (singlet), d (doublet), t (triplet), m (multiplet) and br (broad). IR spectra were measured by an Agilent Technologies 5500 Series FT-IR spectrometer. High-resolution mass spectroscopy (HRMS) spectra were obtained using fast atom bombardment (FAB), electrospray ionization (ESI) and matrix-assisted laser desorption/ionization time of flight (MALDI-TOF). The ball milling experiments were carried out in a Retsch MM400 mill using 10 mL stainless grinding jars (3 stainless steel balls, 7 mm Ø).

General procedure of synthesis of calix[n]triazolium (1–3) by ball milling.

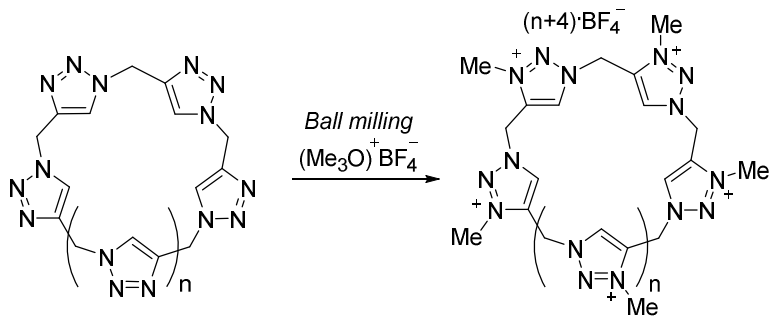

4 (n = 0)
5 (n = 1)
6 (n = 2)

1 (n = 0, 97%)
2 (n = 1, 98%)
3 (n = 2, 95%)

The calix[n]triazole **4**–**6** for the synthesis of calix[n]triazolium **1**–**3** were prepared according to a previously published procedure.[S1] The calix[n]triazole **4**–**6** (0.617mmol, 1 equiv.) and $(Me_3O)^+BF_4^-$ (1.2 equiv. per 1,2,3-triazole unit, *i.e.*, 4.8 equiv. for **4**, 6.0 equiv. for **5** and 7.2 equiv. for **6**) were placed into a 10 mL stainless grinding jar with three stainless balls (7 mm diameter). The reaction mixture was ground at 30 Hz with a vibrational ball mill for 1.5 h at room temperature. The resulting mixtures were diluted with methanol, and the insoluble products were collected by centrifuge. The obtained products were washed with methanol several times by centrifugation. Then, the products were dried overnight via lyophilization.

Calix[4]triazolium (1)

Following the general procedure, the product was collected and purified using centrifugation to yield product **1** (438 mg, 97%) as a white solid; m.p. is not given (decomposition at over 200 °C); ^{1}H NMR ($(CD_3)_2SO$, 400 MHz, single conformer) δ 9.01 (s, 4H), 6.58 (s, 8H), 4.33 (s, 12H) ppm.; ^{13}C NMR ($(CD_3)_2SO$, 100 MHz, single conformer) δ 138.1 (4C), 131.2 (4C), 44.4 (4C), 38.8 (4C) ppm.; IR (neat) υ_{max} 3158, 3125, 3028, 1589, 1458, 1031, 1008, 815 (cm^{-1}); HRMS (FAB) *m/z* calcd for $C_{16}H_{23}B_2F_8N_{12}$ 557.2227 ([M–2BF_4^-–H]$^+$), found 557.2224.

Calix[5]triazolium (2)

Following the general procedure, the product was collected and purified using centrifugation to yield a mixture of conformers of **2** (553 mg, 98%) as a white solid; m.p. is not given (decomposition at over 200 °C); ^{1}H NMR ($(CD_3)_2SO$, 400 MHz, mixture of conformers) δ 9.25 (s, 4.2H), 9.13 (s, 0.4H), 8.93 (s, 0.4H), 6.48–6.43 (m, 10H), 4.38–4.34 (m, 15H) ppm.; ^{13}C NMR ($(CD_3)_2SO$, 100 MHz, mixture of conformers) δ 135.5 (5C, conformer 1), 135.1 (5C, conformer 2), 133.0 (5C, conformer 1), 132.0 (5C, conformer 2), 43.5 (5C, conformer 1), 42.8 (5C, conformer 2), 38.82 (5C, conformer 1), 38.75 (5C, conformer 2) ppm.; IR (neat) υ_{max} 3131, 3032, 1590, 1453, 1330, 1021, 818 (cm^{-1}); HRMS (FAB) *m/z* calcd for $C_{20}H_{29}B_3F_{12}N_{15}$ 740.2818 ([M–2BF_4^-–H]$^+$), found 740.2827.

Calix[6]triazolium (3)

Following the general procedure, the product was collected and purified using centrifugation to yield a mixture of conformers of **3** (643 mg, 95%) as a white solid; m.p. is not given (decomposition at over 200 °C); ^{1}H NMR ($(CD_3)_2SO$, 600 MHz, mixture of conformers) δ 9.26–9.25 (m, 6H), 6.50–6.48 (m, 12H), 4.34 (s, 7.2H), 4.19 (s, 10.8H) ppm.; ^{13}C NMR ($(CD_3)_2SO$, 100 MHz, mixture of conformers) δ 135.6 (6C, conformer 1), 135.2 (6C, conformer 2), 133.2 (6C, conformer 1), 132.8 (6C, conformer 2), 43.6 (6C, conformer 1), 43.3 (6C, conformer 2), 38.6 (12C, conformers) ppm.; IR (neat) υ_{max} 3130, 3037, 2988, 1593, 1453, 1329, 1023, 820 (cm^{-1}); MALDI−TOF MS (Matrix: dithranol) *m/z* calcd for $C_{24}H_{33}B_2F_8N_{18}$ 747.3194 ([M–4BF_4^-–3H]$^+$), found 747.1875.

Synthesis of sodium salt of chromenolate 7$^-$.

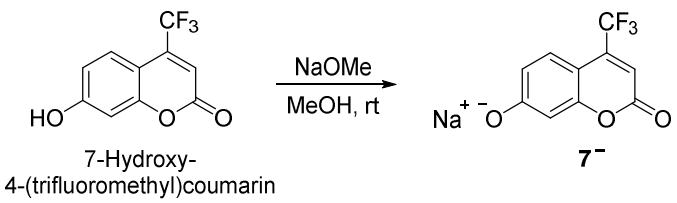

7-Hydroxy-
4-(trifluoromethyl)coumarin

7$^-$

Commercially available 7-hydroxy-4-(trifluoromethyl)coumarin (300 mg, 1.30 mmol), dissolved in MeOH (30 mL), was added to NaOMe (70.0 mg, 1.30 mmol), dissolved in MeOH (30 mL). After the addition was complete, stirring was continued for 30 min at room temperature. Then, the organic layer was evaporated *in vacuo* and the residue was washed with Et_2O. The obtained solid was dried under high vacuum to produce the desired product **7**$^{-}$ (260 mg, 79%) as a yellow solid; m.p. is not given (decomposition at over 200 °C); ^{1}H NMR ($(CD_3)_2SO$, 400 MHz) δ 7.10–7.07 (m, 1H), 6.16 (dd, J = 9.2, 2.2 Hz, 1H), 5.93 (d, J = 2.3 Hz, 1H), 5.78 (s, 1H) ppm.; ^{13}C NMR ($(CD_3)_2SO$, 100 MHz) δ 177.5, 160.9, 158.8, 140.4 (q, J = 30.3 Hz), 124.6 (d, J = 1.4 Hz), 122.7 (q, J = 274.4 Hz), 120.6, 104.1, 97.44, 97.35 ppm.; IR (neat) υ_{max} 2832, 1684, 1582, 1432, 1364, 1282, 1193, 1132, 843, 724 (cm^{-1}); HRMS (ESI) m/z calcd for $C_{10}H_4F_3O_3$ 229.0107 ([M–Na^{+}]$^{+}$), found 229.0108.

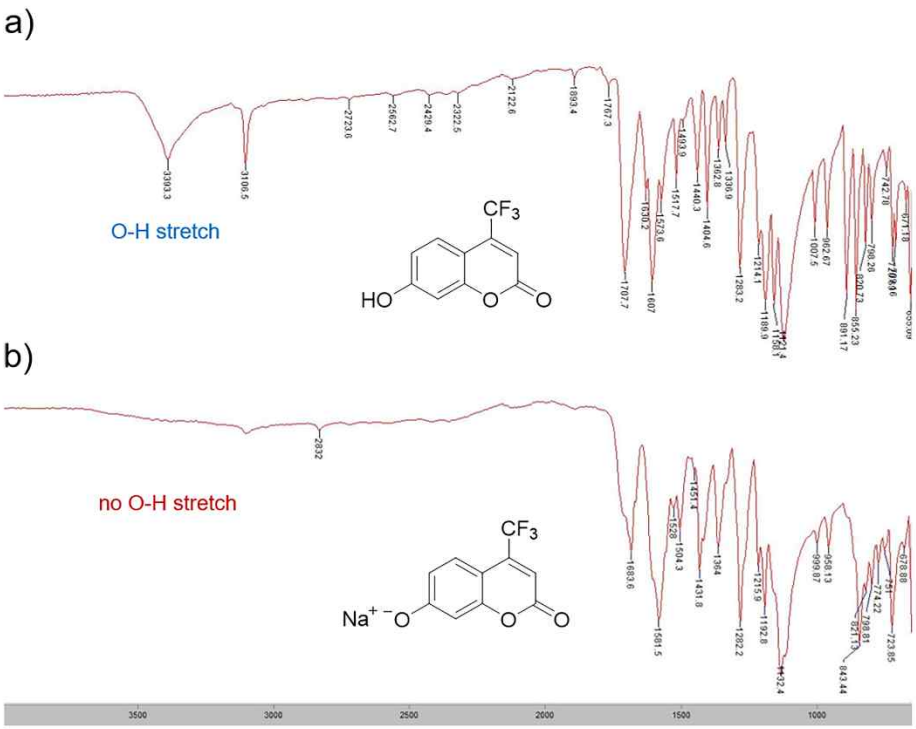

Figure S1. IR spectra of (a) 7-hydroxy-4-(trifluoromethyl)coumarin and (b) its sodium salt **7**$^{-}$. The disappearance of broad band at 3393 cm^{-1} of spectrum (b) indicates complete ionization of 7-hydroxy-4-(trifluoromethyl)coumarin.

2. X-Ray crystallographic data

Single crystal X-ray diffraction analysis. X-ray data for single crystals of **1** were recorded with a cryoloop mounted on a goniometer head in a cold stream of liquid nitrogen. The diffraction data were measured with synchrotron radiation with a Rayonix MX225HS CCD area detector with a silicon (111) double-crystal monochromator at the Pohang Accelerator Laboratory, Korea. The PAL BL2D-SMDC program[S2] was used for data collection and HKL3000sm[S3] was used for cell refinement, reduction, and absorption correction. The structure was solved by direct methods and refined by full-matrix least-squares analysis using anisotropic thermal parameters for non-hydrogen atoms with the SHELXTL program. All hydrogen atoms were calculated at idealized positions and refined with the riding models. CCDC2057514 (**1**) contains the supplementary crystallographic data for this paper.

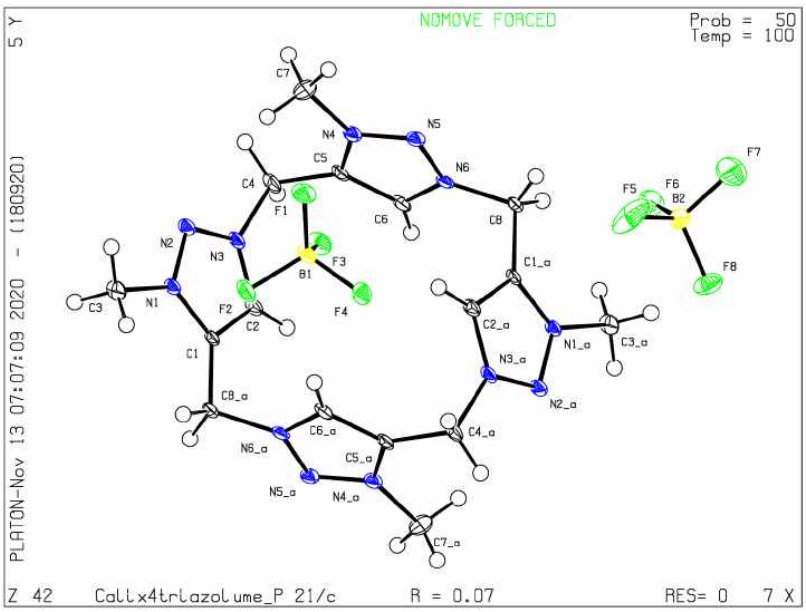

Figure S2. X-ray crystal structure of **1**. CCDC 2057514 (**1**) contains the supplementary crystallographic data for this paper. These data can be obtained free of charge from the Cambridge Crystallographic Data Centre via www.ccdc.cam.ac.uk/data_request/cif.

Table S1. Crystal data and structure refinement for **1**.

Identification code	Calix[4]triazolume_BF4	
Empirical formula	C16 H24 B4 F16 N12	
Formula weight	731.71	
Temperature	100(2) K	
Wavelength	0.700 Å	
Crystal system	Monoclinic	
Space group	$P2_1/c$	
Unit cell dimensions	a = 10.501(2) Å	α= 90°.
	b = 10.032(2) Å	β= 106.55(3)°.
	c = 13.491(3) Å	γ = 90°.
Volume	1362.3(5) $Å^3$	
Z	2	
Density (calculated)	1.784 Mg/m^3	
Absorption coefficient	0.179 mm^{-1}	
F(000)	736	
Crystal size	0.151 x 0.112 x 0.049 mm^3	
Theta range for data collection	2.531 to 33.512°.	
Index ranges	-16<=h<=16, -14<=k<=14, -20<=l<=20	
Reflections collected	11442	
Independent reflections	4329 [R(int) = 0.1026]	
Completeness to theta = 24.835°	90.3 %	
Absorption correction	Empirical	
Max. and min. transmission	1.000 and 0.609	
Refinement method	Full-matrix least-squares on F^2	
Data / restraints / parameters	4329 / 0 / 219	
Goodness-of-fit on F^2	1.110	
Final R indices [I>2sigma(I)]	R1 = 0.0729, wR2 = 0.2099	
R indices (all data)	R1 = 0.0751, wR2 = 0.2119	
Extinction coefficient	n/a	
Largest diff. peak and hole	0.741 and -0.654 $e.Å^{-3}$	

3. DFT calculation for conformational study

General methods. To investigate conformational stability for calix[n]triazoliums (**1**–**3**), density functional theory (DFT) calculations were performed, using the ωB97xD functional, comprising a version of Grimme's D2 dispersion model, at the 6-31++G(d,p) level of theory.[S4] All calculations were performed using the Gaussian 16W program package.[S5] Input file generation was performed using Gabedit 2.5.0.[S6]

Table S2. The calculated heat of formation (in kcal/mol), and their relative energies (in parenthesis) and optimized geometries for possible conformers of calix[4]triazolium (**1**).

Conformers	*Cone*	*Partial cone*	*1,2-alternate*	*1,3-alternate*
Top view	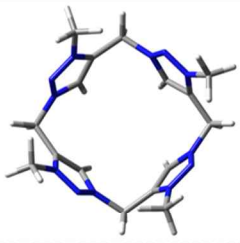	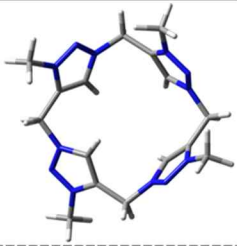	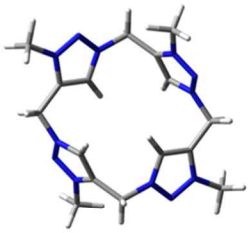	
Side view	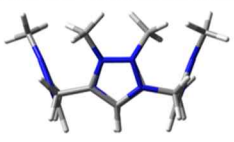	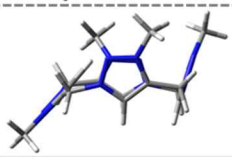	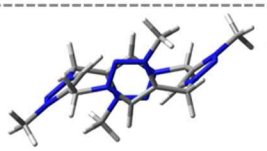	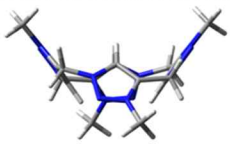
Energy	-802702.32900183 (0.09331068)	-802702.2252117 (0.19710081)	-802702.42231251 (0.00000000)	-802702.21178304 (0.21052947)

Table S3. The calculated heat of formation (in kcal/mol), and their relative energies (in parenthesis) and optimized geometries for possible conformers of calix[5]triazolium (**2**).

Conformers	*Cone*	*Partial cone*	*1,2-alternate*	*1,3-alternate*
Top view	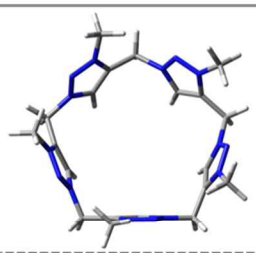	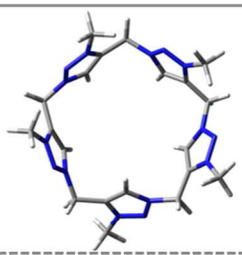	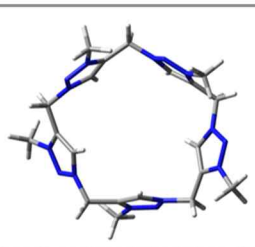	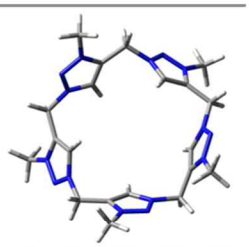
Side view	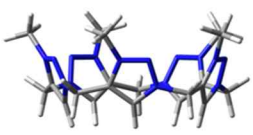	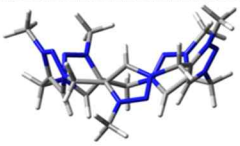	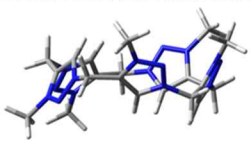	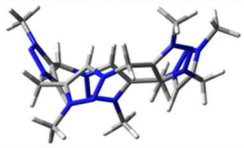
Energy	*-1003301.659234 (0.000000)*	*-1003299.795405 (1.863829)*	*-1003300.0687482 (1.5904858)*	*-1003298.142545 (3.516689)*

Table S4. The calculated heat of formation (in kcal/mol), and their relative energies (in parenthesis) and optimized geometries for possible conformers of calix[6]triazolium (**3**).

Conformers	*Cone*	*Partial cone*	*1,2-alternate*	*1,3-alternate*
Top view	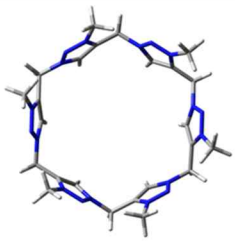	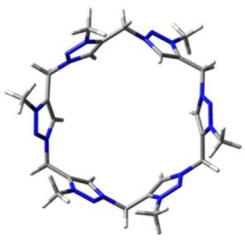	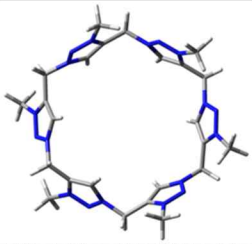	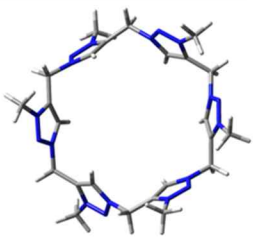
Side view	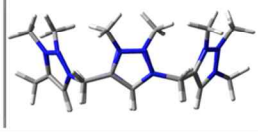	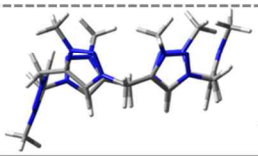	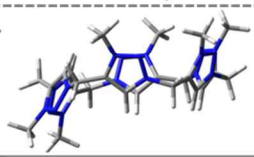	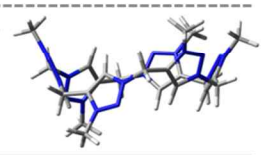
Energy	*-1203878.3088217 (0.000000)*	*-1203874.8892708 (3.4195509)*	*-1203875.2005156 (3.1083061)*	*-1203871.6013715 (6.7074502)*
Conformers	***1,4-alternate***	***1,2,3-alternate***	***1,2,4-alternate***	***1,3,5-alternate***
Top view	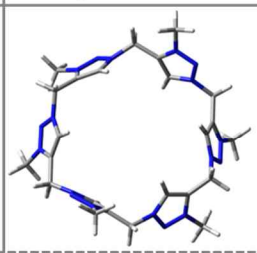	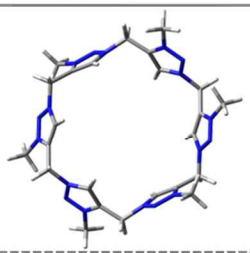	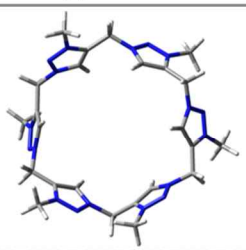	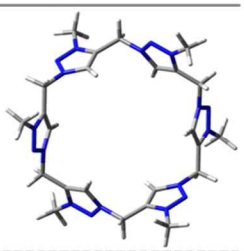
Side view	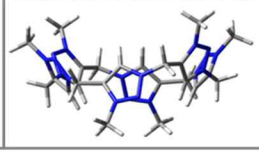	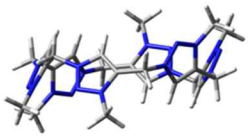	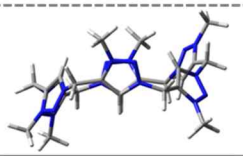	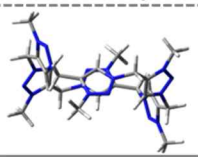
Energy	*-1203871.8910927 (6.417729)*	*-1203875.143475 (3.1653467)*	*-1203871.9363361 (6.3724856)*	*-1203868.399127 (9.9096947)*

4. ^{1}H NMR studies of calix[n]triazoliums

(1) ^{1}H NMR of calix[n]triazoliums (1–3)

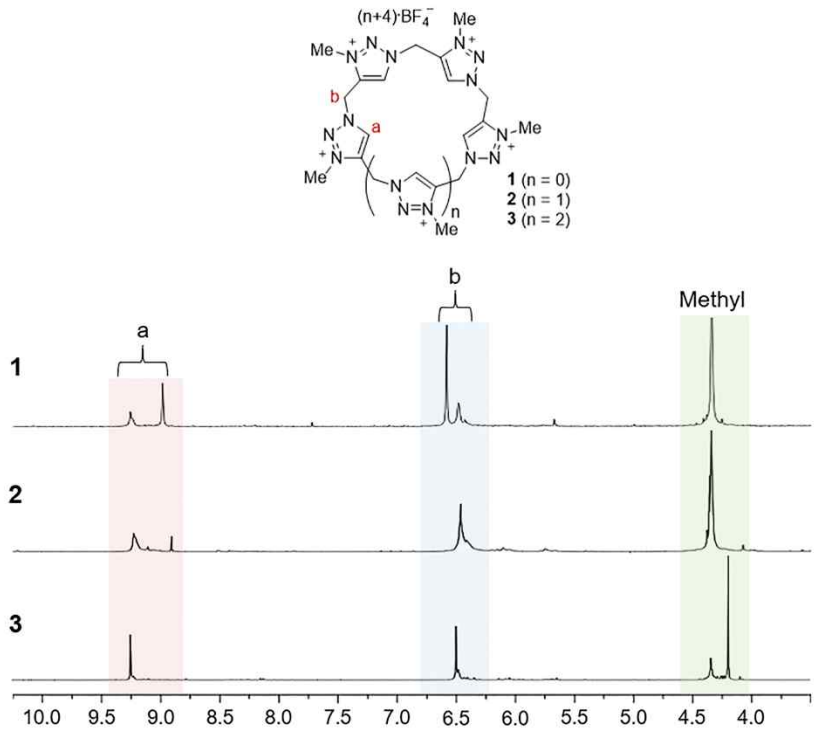

Figure S3. ^{1}H NMR spectrum of **1**–**3** in DMSO-d_6.

(2) Variable-temperature (VT) ^{1}H-NMR studies

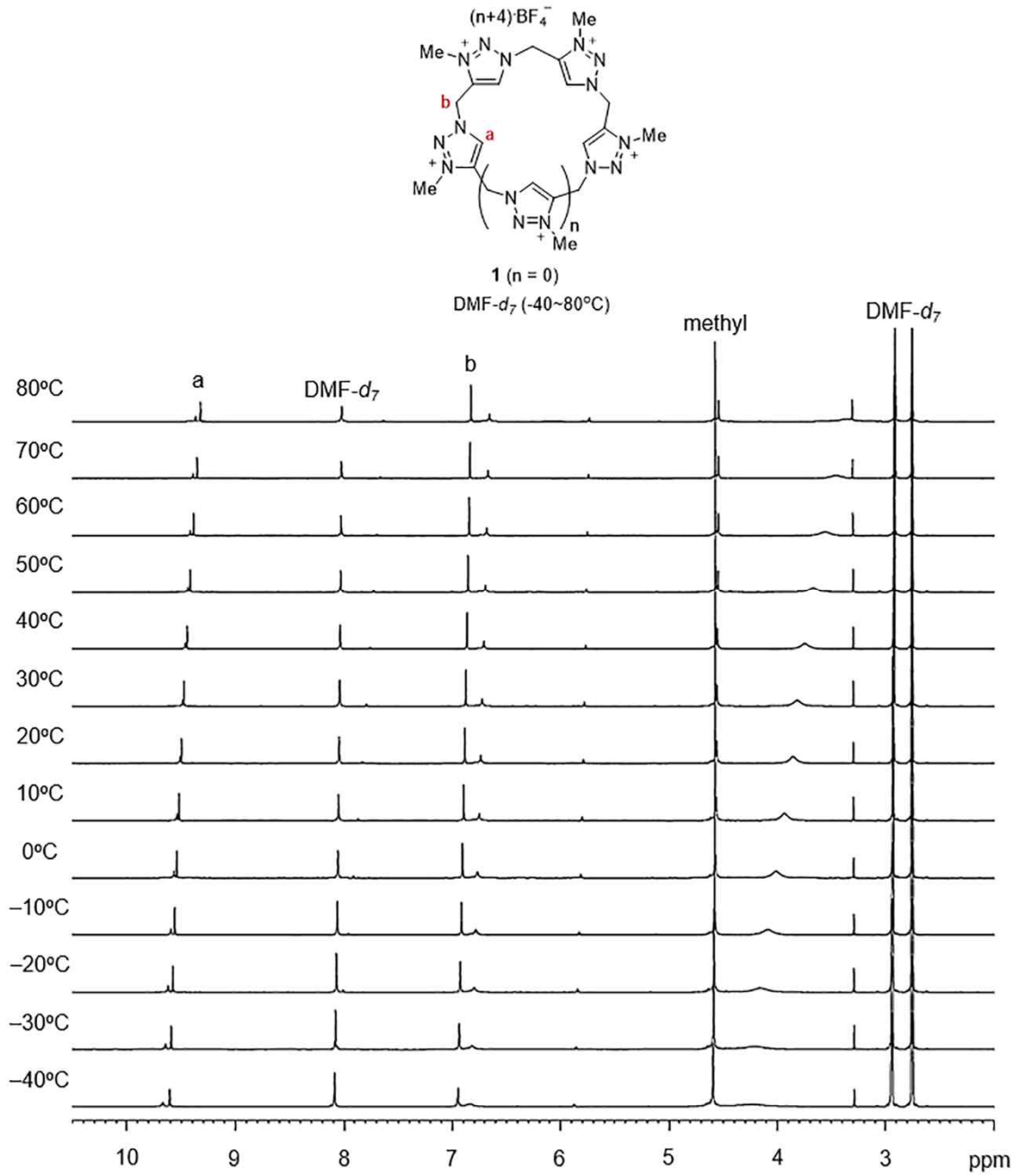

Figure S4. ^{1}H NMR Spectra of **1** in DMF-d_7 at different temperatures (–40 ~ 80 °C).

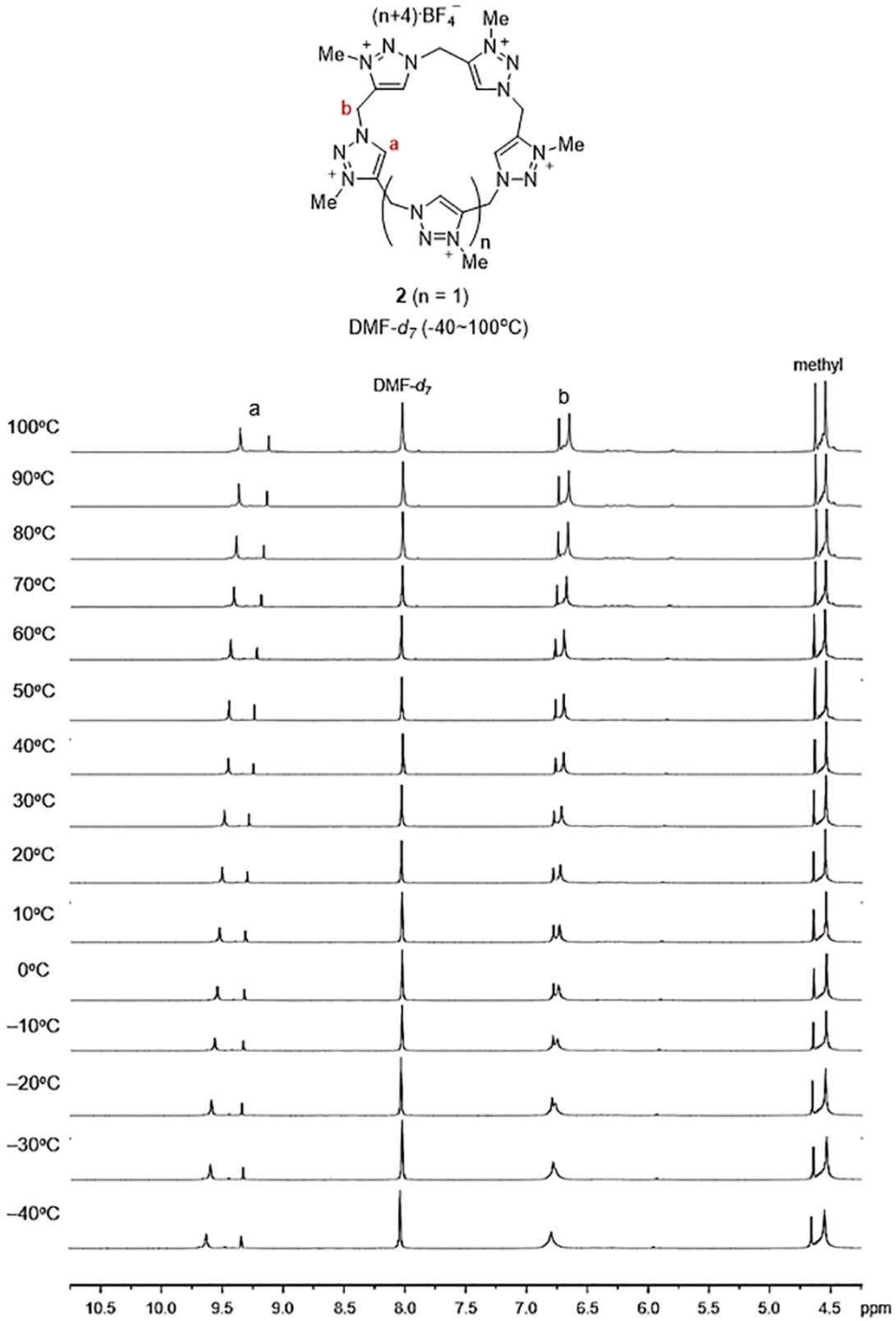

Figure S5. ^{1}H NMR Spectra of **2** in DMF-d_7 at different temperatures (–40 ~ 100 °C).

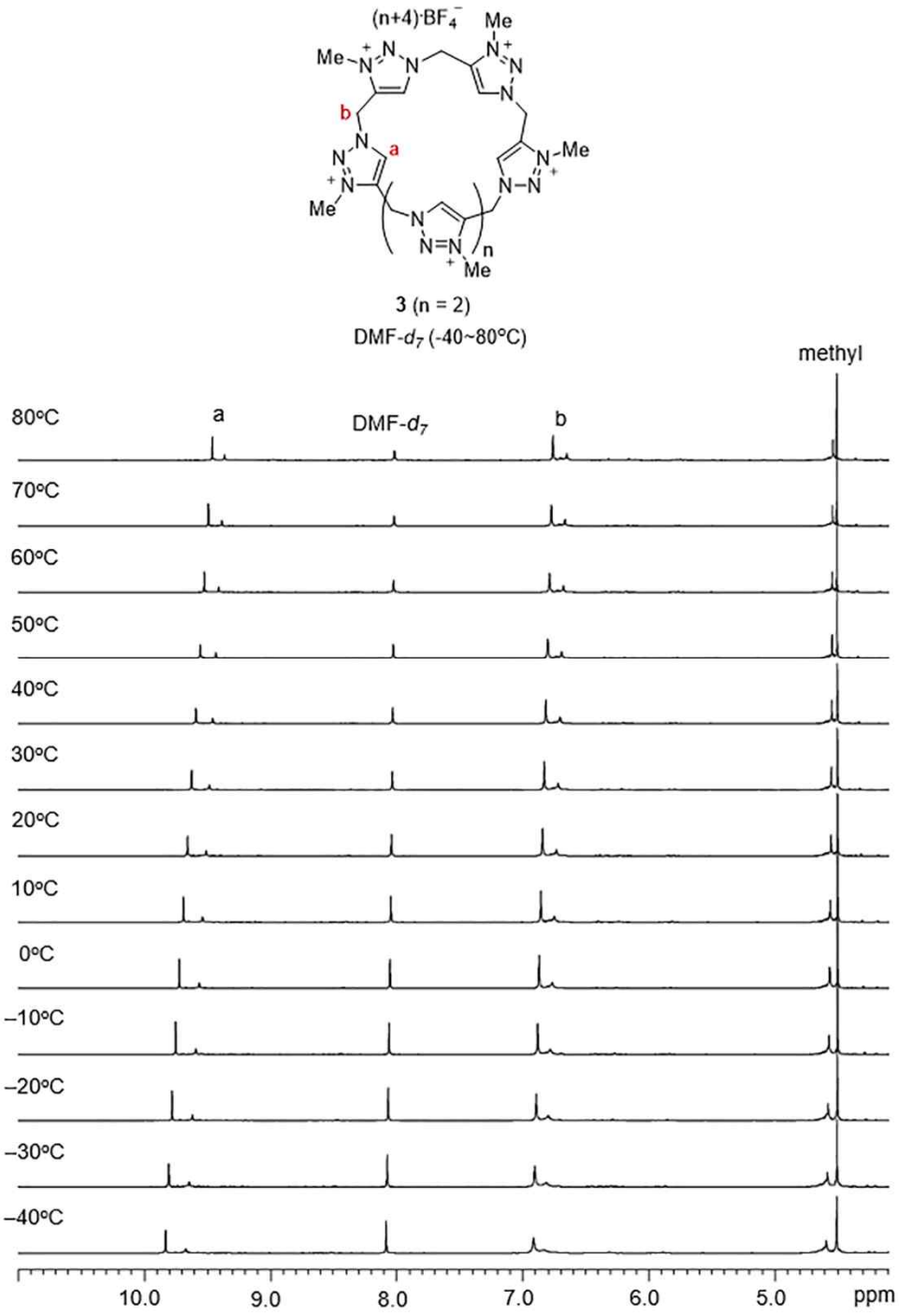

Figure S6. ^{1}H NMR Spectra of **3** in DMF-d_7 at different temperatures (–40 ~ 80 °C).

(3) Hydrogen/deuterium (H/D) exchange of calix[n]triazoliums (1–3)

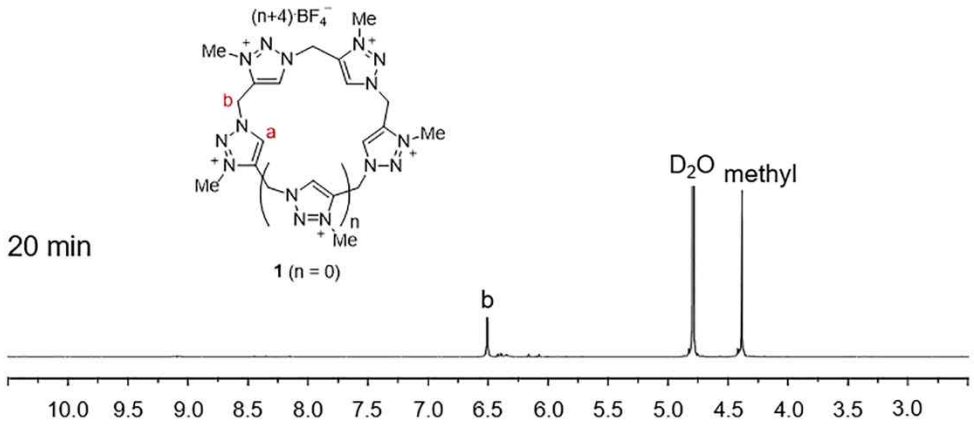

Figure S7. ^{1}H NMR Spectra of **1** in D_2O. Triazolium protons (H_a) disappeared within 20 min.

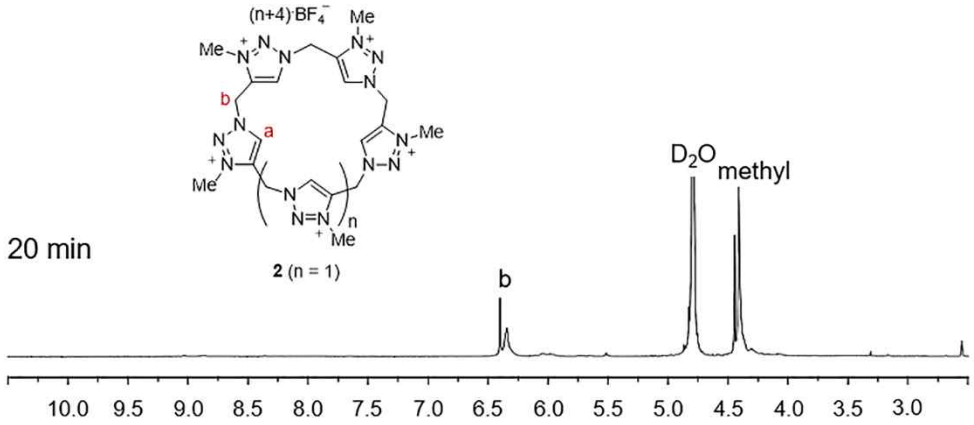

Figure S8. ^{1}H NMR Spectra of **2** in D_2O. Triazolium protons (H_a) disappeared within 20 min.

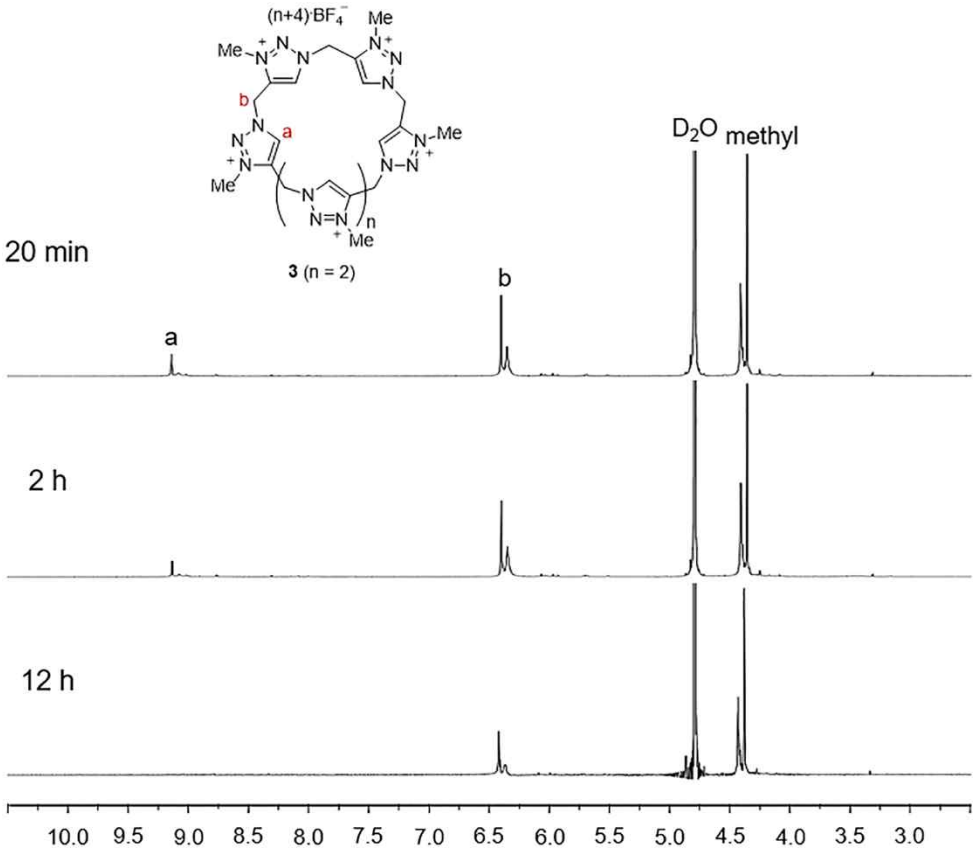

Figure S9. ^{1}H NMR Spectra of **3** in D_2O. Triazolium protons (H_a) disappeared within 12 h.

5. Complexation studies between calix[n]triazoliums and chromenolate

(1) Fluorescence titration of calix[n]triazoliums **1–3** with chromenolate **7**$^{-}$: Stock solutions of calix[n]triazoliums **1–3** (50 mM) and chromenolate **7**$^{-}$ (10 μM) in water were prepared separately. A 3 mL **7**$^{-}$ solution was transferred to a cuvette and an initial spectrum was taken. Aliquots of **1–3** solutions (0–20 μL) were added to the cuvette and the spectrum was recorded after each addition. The binding constant was analyzed by Bindfit, plotting fluorescence emission values at 500 nm against equivalents of the **1–3** added. The graph of the fluorescence titration of chromenolate **7**$^{-}$ using **3** is shown in Fig. 2 in the manuscript.

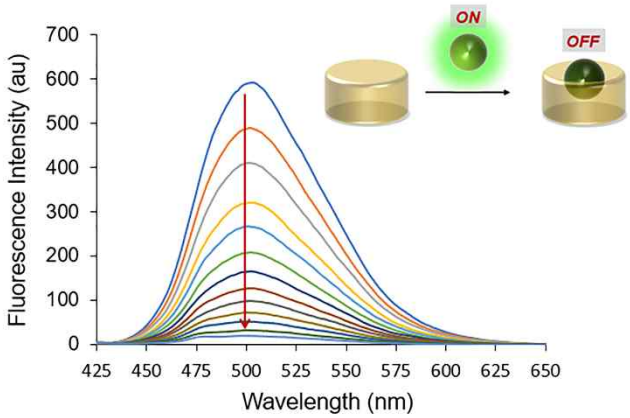

Figure S10. Fluorescence spectra of **7**$^{-}$ (10 μM) upon titration with **1** (0–10 μL) in water (λ_{ex} = 410 nm).

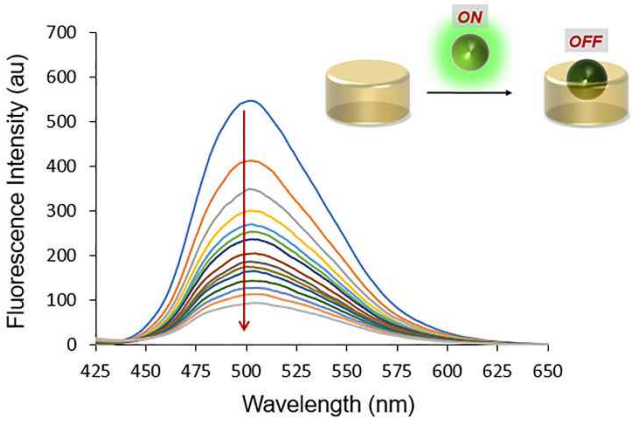

Figure S11. Fluorescence spectra of **7**$^{-}$ (10 μM) upon titration with **2** (0–12 μL) in water (λ_{ex} = 410 nm).

(2) Job's plot for the binding stoichiometric ratio: Stock solutions of equal concentration of calix[n]triazoliums **1–3** (10 μM) and chromenolate **7**$^{-}$ (10 μM) in water were prepared separately. Ten vials were each filled with a total 10 mL solution of calix[n]triazoliums **1–3** and chromenolate **7**$^{-}$ in the following ratios (**1–3**:**7**$^{-}$): 10:0, 9:1, 8:2, 7:3, 6:4, 5:5, 4:6, 3:7, 2:8, 1:9. Job's plot was constructed by plotting the change in fluorescence at 500nm of chromenolate **7**$^{-}$ against the molar fraction of the host.

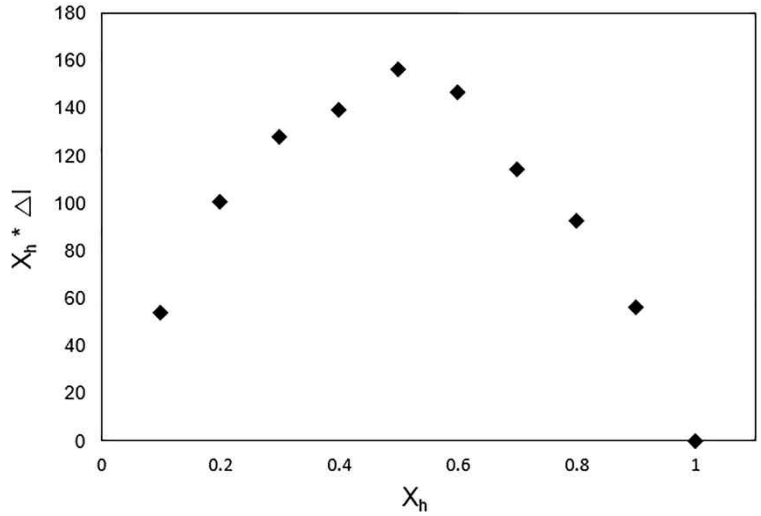

Figure S12. Job's plot generated from the fluorescence titration data of **1** with **7**$^{-}$ in water.

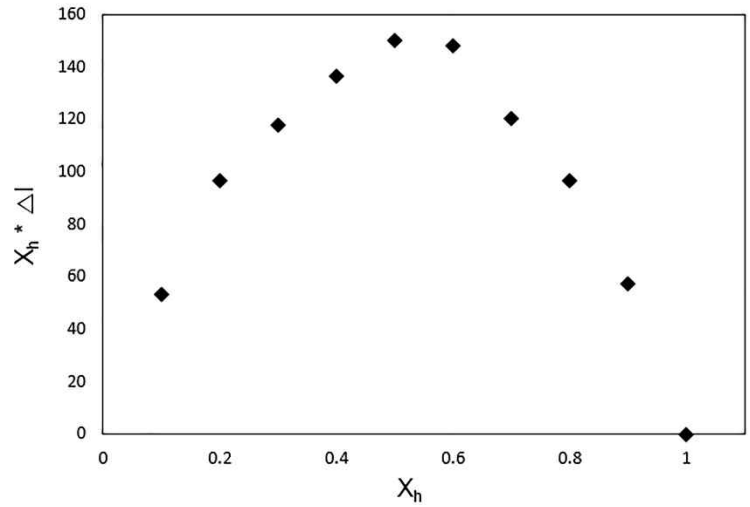

Figure S13. Job's plot generated from the fluorescence titration data of **2** with **7**$^{-}$ in water.

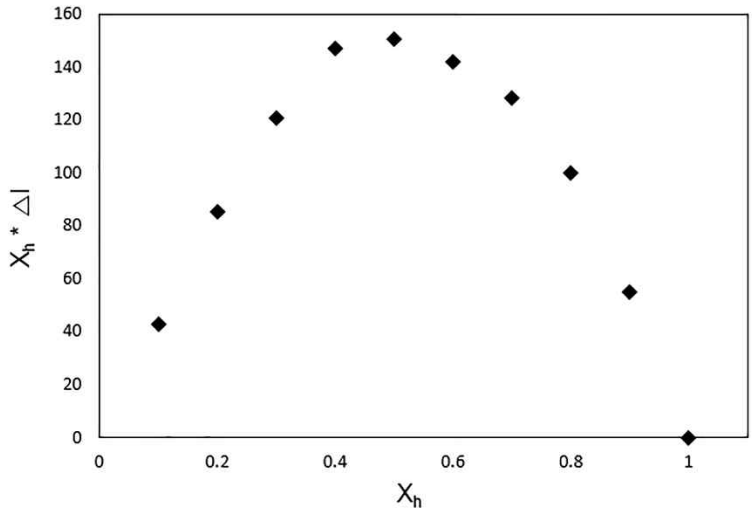

Figure S14. Job's plot generated from the fluorescence titration data of **3** with **7**$^{-}$ in water.

(3) Association constant calculated by bindfit

a. Association constant of **1**/**7**$^{-}$ complex

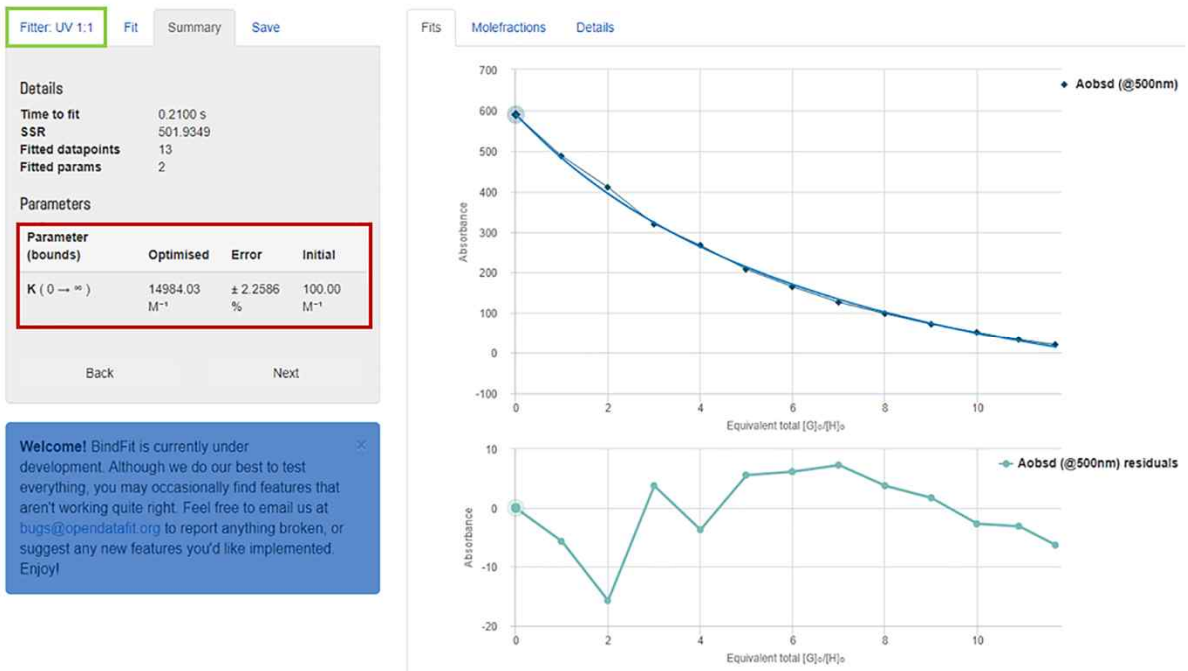

Figure S15. Screenshot of the summary window of http://app.supramolecular.org/bindfit/. This screenshot shows the raw data for fluorescence titration of **7**$^{-}$ with **1** following the fluorescence emission values at 500 nm vs. the data fitted to 1 : 1 UV binding model, the corresponding residual plot and the association constants with the calculated asymptotic standard errors.

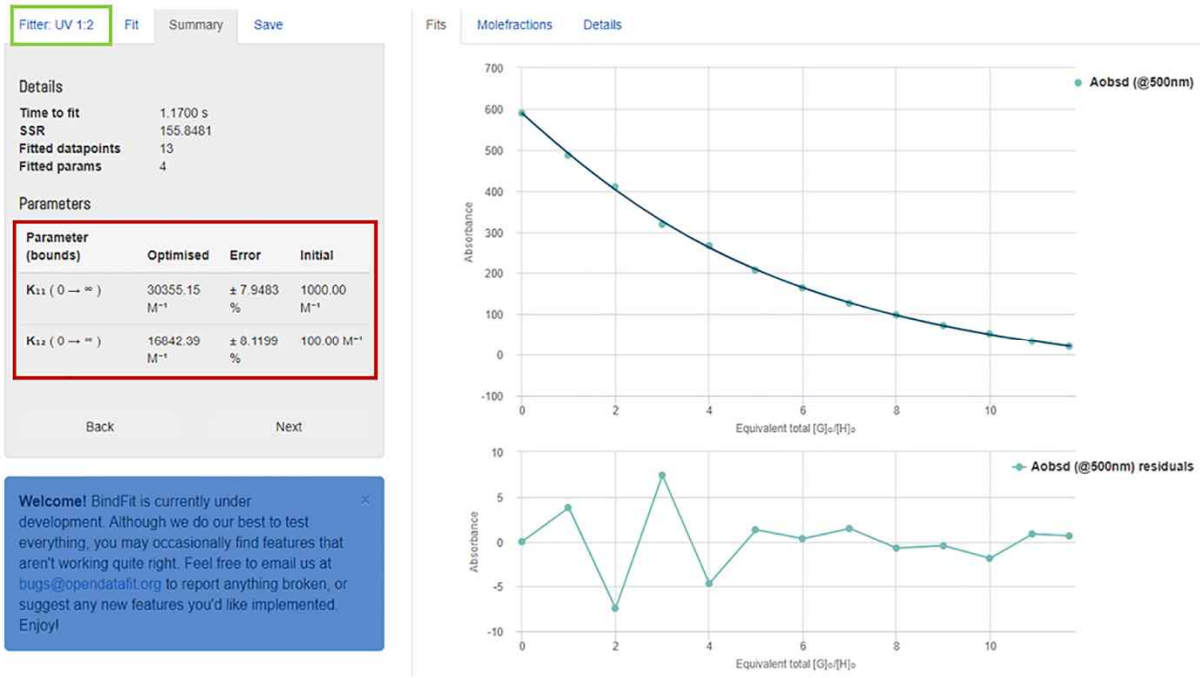

Figure S16. Screenshot of the summary window of http://app.supramolecular.org/bindfit/. This screenshot shows the raw data for fluorescence titration of **7**$^{-}$ with **1** following the fluorescence emission values at 500 nm vs. the data fitted to 1 : 2 UV binding model, the corresponding residual plot and the association constants with the calculated asymptotic standard errors.

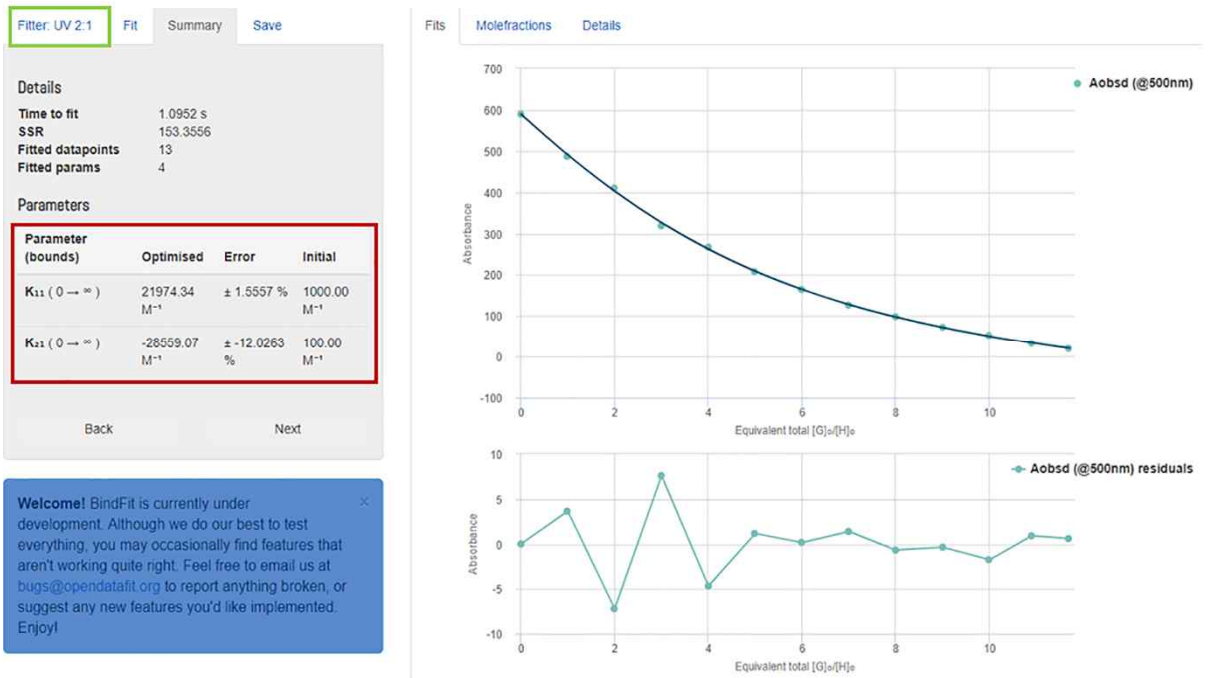

Figure S17. Screenshot of the summary window of http://app.supramolecular.org/bindfit/. This screenshot shows the raw data for fluorescence titration of **7**$^{-}$ with **1** following the fluorescence emission values at 500 nm vs. the data fitted to 2 : 1 UV binding model, the corresponding residual plot and the association constants with the calculated asymptotic standard errors.

Table S5. Summary of association constants between **1** and **7**$^{-}$ according to different binding models.[a]

Binding models		
1 : 1	1 : 2	2 : 1
14984.03 (±2.26%)	K_{11} 30355.15 (±7.95) K_{12} 16842.39 (±8.12%)	K_{11} 21974.34 (±1.56) K_{21} -28559.07 (±-12.03%)

[a] The Bindfit software for data analysis was used from *supramolecular.org*.

b. Association constant of **2**/**7**$^{-}$ complex

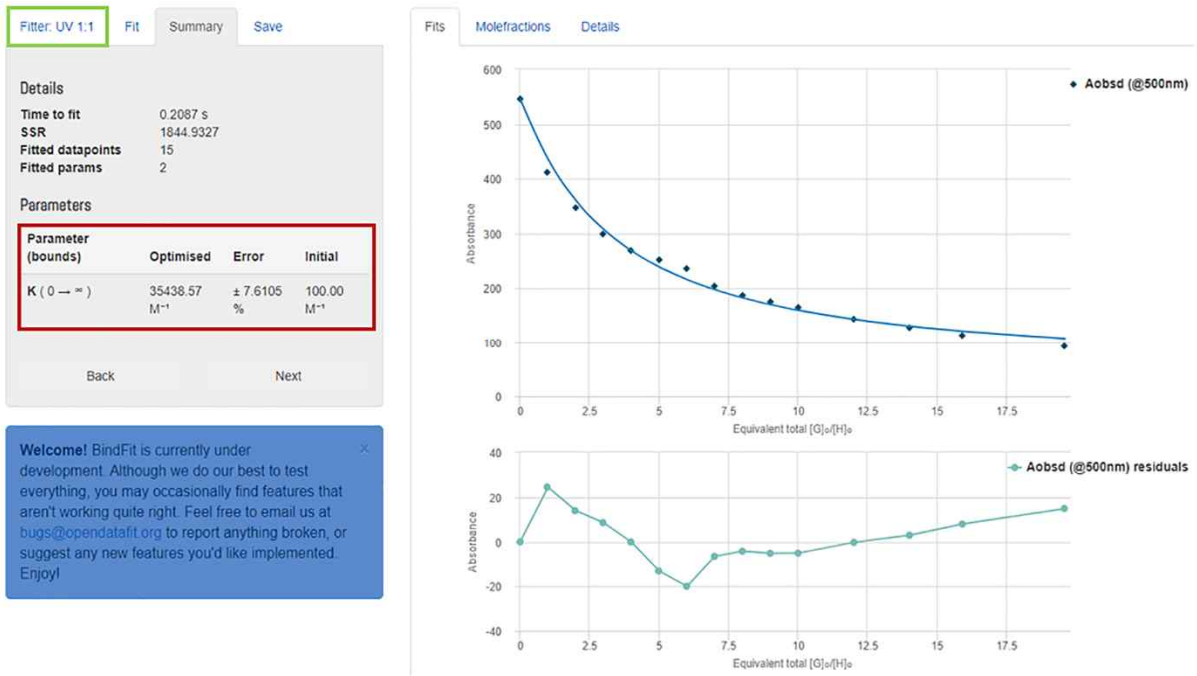

Figure S18. Screenshot of the summary window of http://app.supramolecular.org/bindfit/. This screenshot shows the raw data for fluorescence titration of **7**$^{-}$ with **2** following the fluorescence emission values at 500 nm vs. the data fitted to 1 : 1 UV binding model, the corresponding residual plot and the association constants with the calculated asymptotic standard errors.

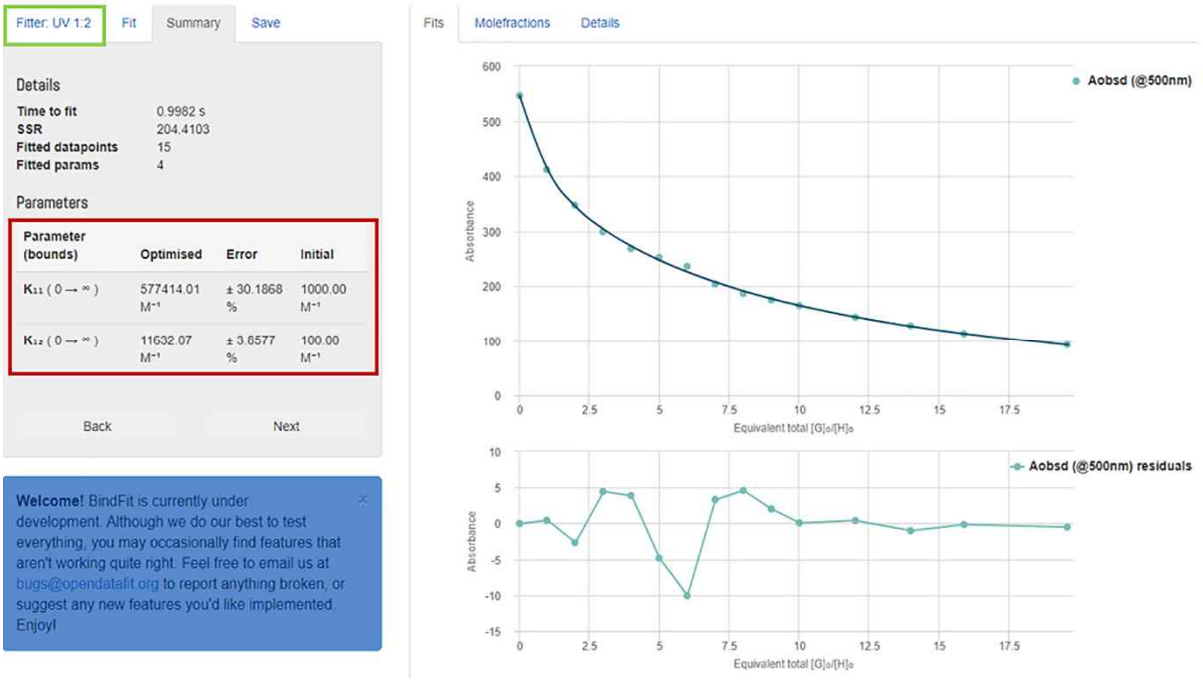

Figure S19. Screenshot of the summary window of http://app.supramolecular.org/bindfit/. This screenshot shows the raw data for fluorescence titration of **7**$^{-}$ with **2** following the fluorescence emission values at 500 nm vs. the data fitted to 1 : 2 UV binding model, the corresponding residual plot and the association constants with the calculated asymptotic standard errors.

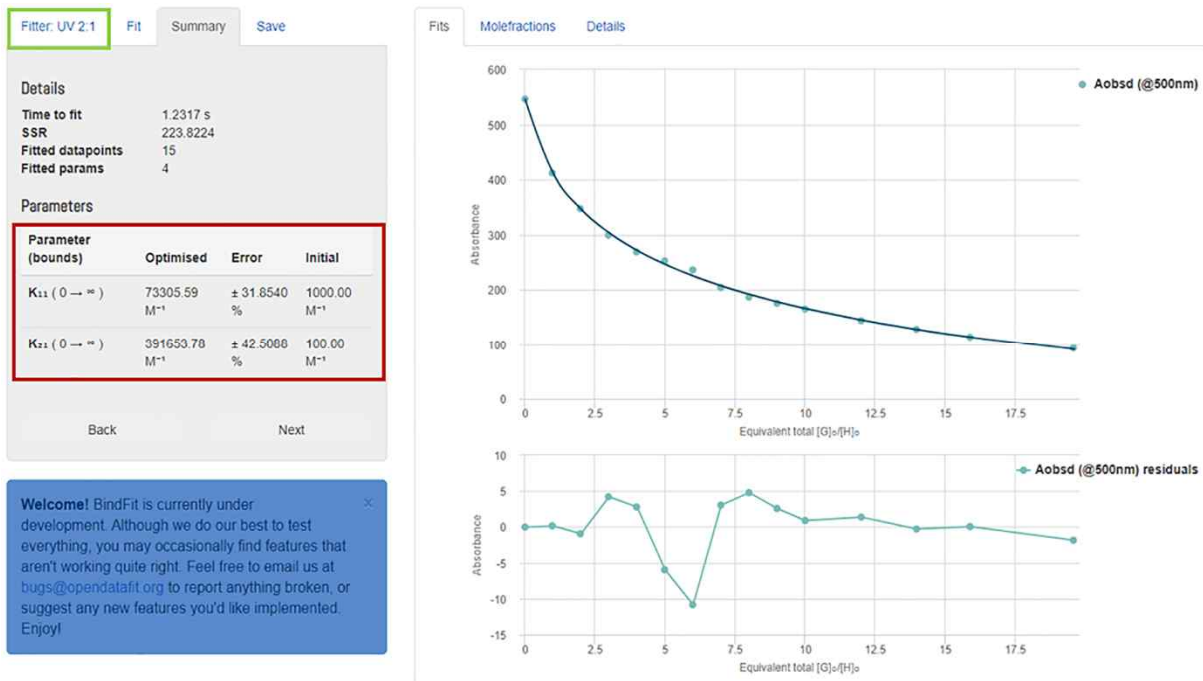

Figure S20. Screenshot of the summary window of http://app.supramolecular.org/bindfit/. This screenshot shows the raw data for fluorescence titration of **7**$^{-}$ with **2** following the fluorescence emission values at 500 nm vs. the data fitted to 2 : 1 UV binding model, the corresponding residual plot and the association constants with the calculated asymptotic standard errors.

Table S6. Summary of association constants between **2** and 7^- according to different binding models.[a]

Binding models		
1 : 1	1 : 2	2 : 1
35438.57 (±7.61%)	K_{11} 577414.01 (±30.19) K_{12} 11632.07 (±3.86%)	K_{11} 73305.59 (±31.85) K_{21} 391653.78 (±42.51%)

[a] The Bindfit software for data analysis was used from *supramolecular.org*.

c. Association constant of **3**/7^- complex

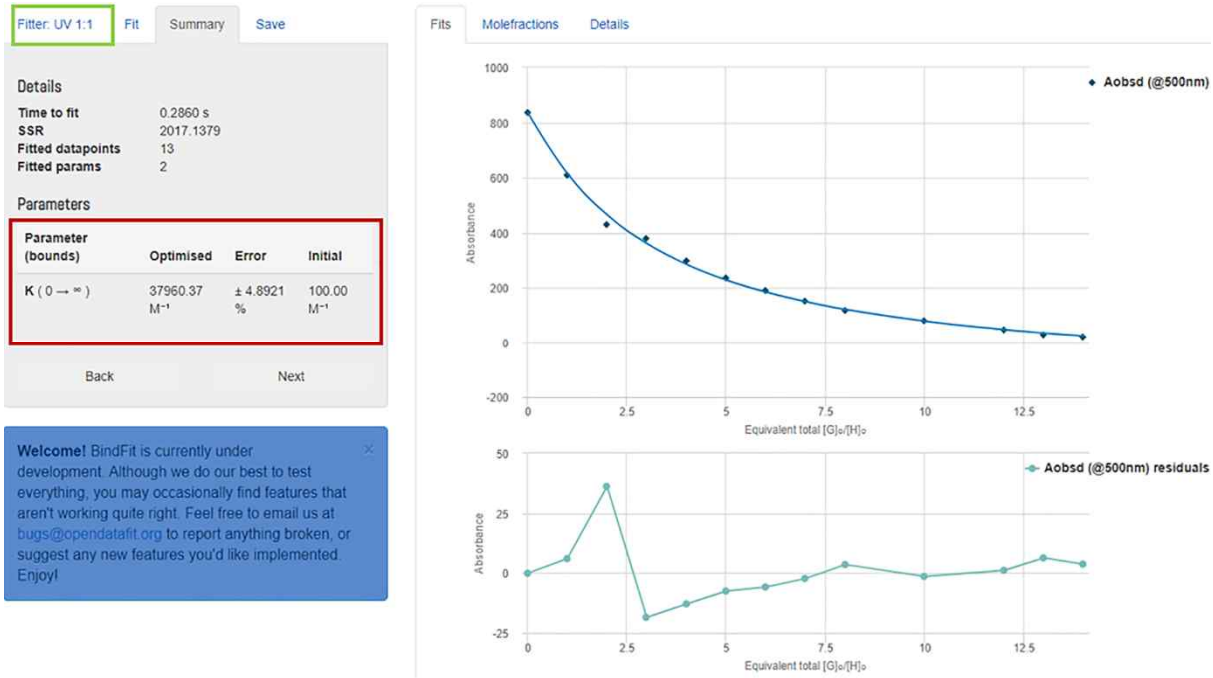

Figure S21. Screenshot of the summary window of http://app.supramolecular.org/bindfit/. This screenshot shows the raw data for fluorescence titration of 7^- with **3** following the fluorescence emission values at 500 nm vs. the data fitted to 1 : 1 UV binding model, the corresponding residual plot and the association constants with the calculated asymptotic standard errors.

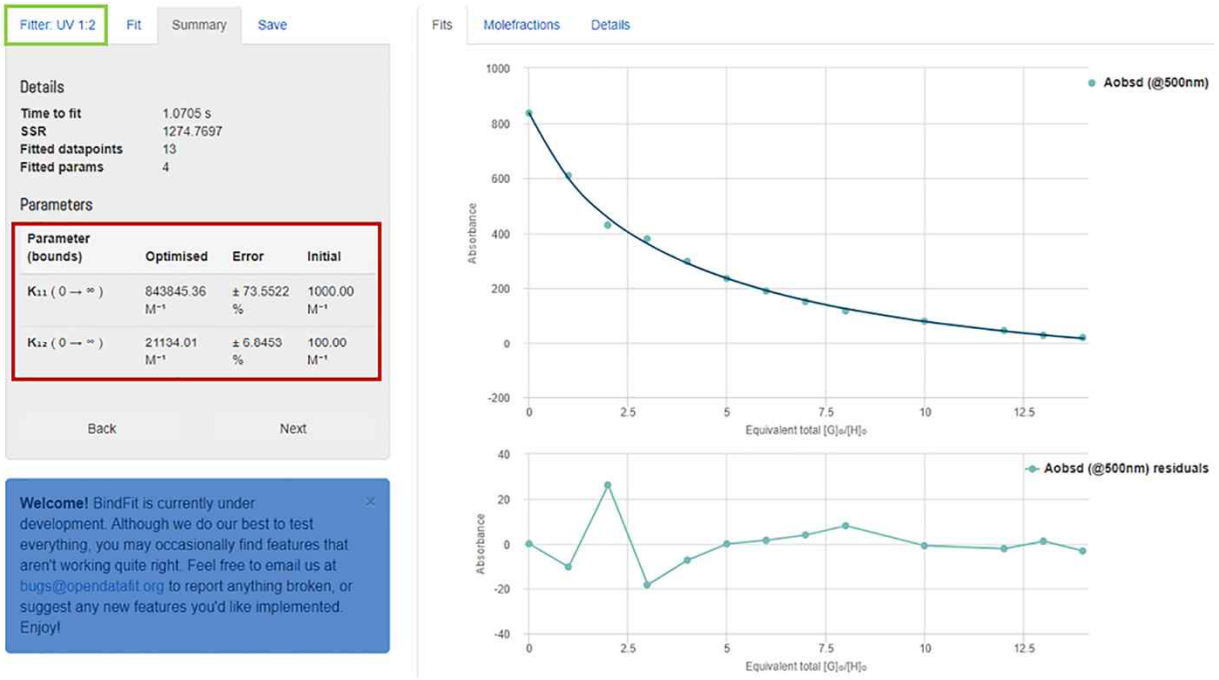

Figure S22. Screenshot of the summary window of http://app.supramolecular.org/bindfit/. This screenshot shows the raw data for fluorescence titration of **7**$^{-}$ with **3** following the fluorescence emission values at 500 nm vs. the data fitted to 1 : 2 UV binding model, the corresponding residual plot and the association constants with the calculated asymptotic standard errors.

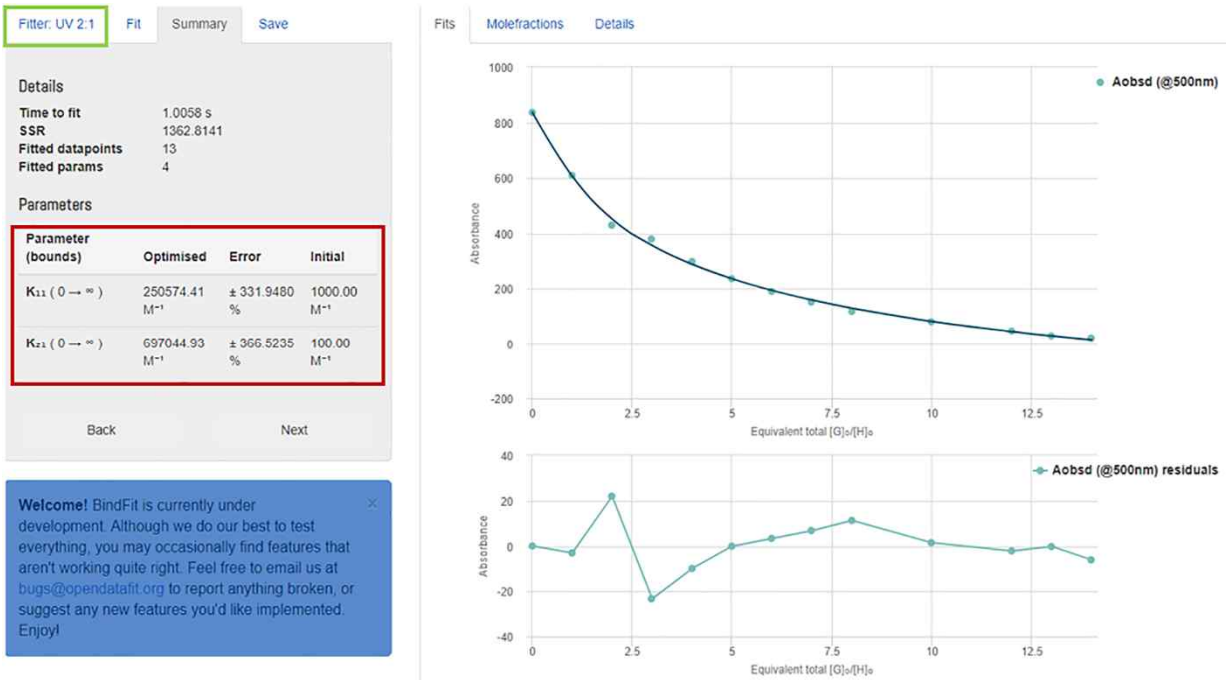

Figure S23. Screenshot of the summary window of http://app.supramolecular.org/bindfit/. This screenshot shows the raw data for fluorescence titration of **7**$^{-}$ with **3** following the fluorescence emission values at 500 nm vs. the data fitted to 2 : 1 UV binding model, the corresponding residual plot and the association constants with the calculated asymptotic standard errors.

Table S7. Summary of association constants between **3** and **7**$^{-}$ according to different binding models.[a]

Binding models		
1 : 1	1 : 2	2 : 1
37960.37 (±4.89%)	K_{11} 843845.36 (±73.55) K_{12} 21134.01 (±6.85%)	K_{11} 250574.41 (±331.95) K_{21} 697044.93 (±366.52%)

[a] The Bindfit software for data analysis was used from *supramolecular.org*.

(4) ^{1}H NMR spectra of **1–3** in the presence of increasing concentrations of **7**$^{-}$

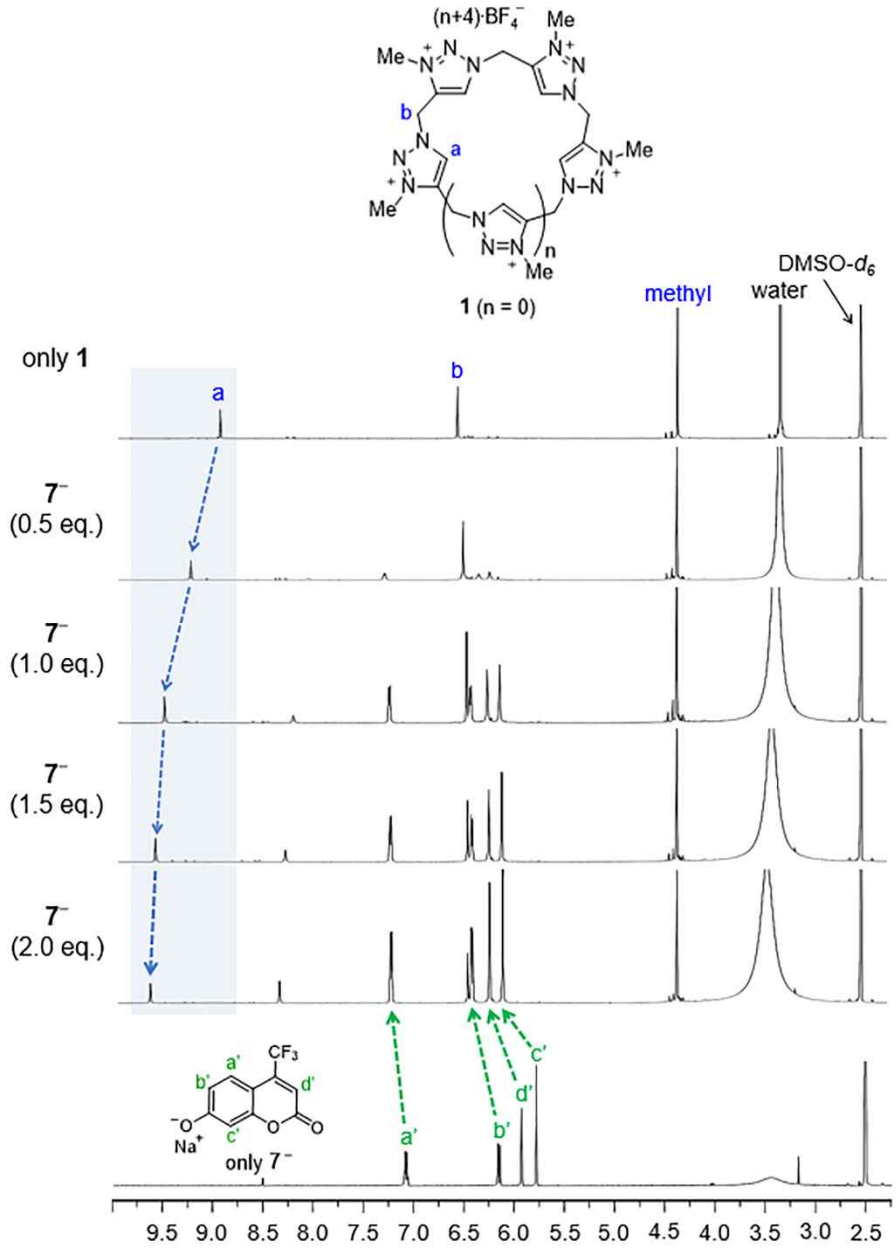

Figure S24. ^{1}H NMR spectra of **1** (2 mM) in DMSO-d_6 recorded in the presence of increasing concentrations of **7**$^{-}$.

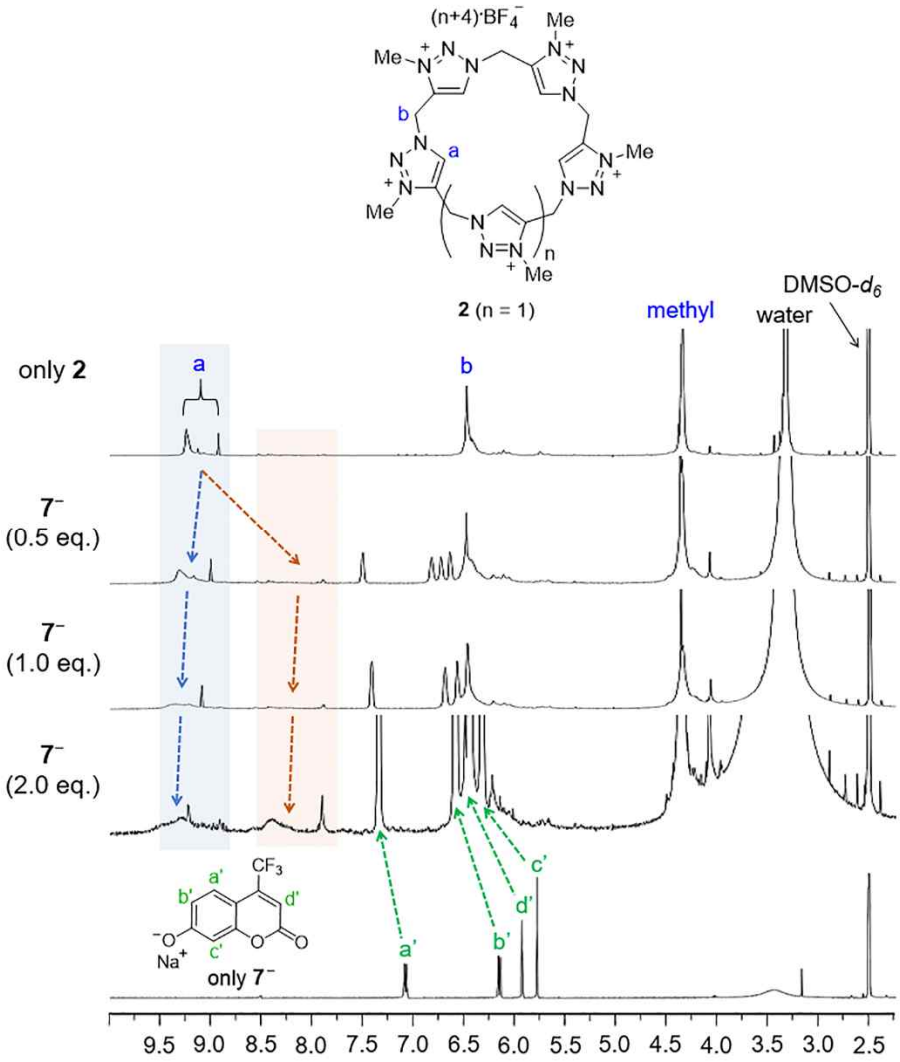

Figure S25. ^{1}H NMR spectra of **2** (2 mM) in DMSO-d_6 recorded in the presence of increasing concentrations of $\mathbf{7}^{-}$.

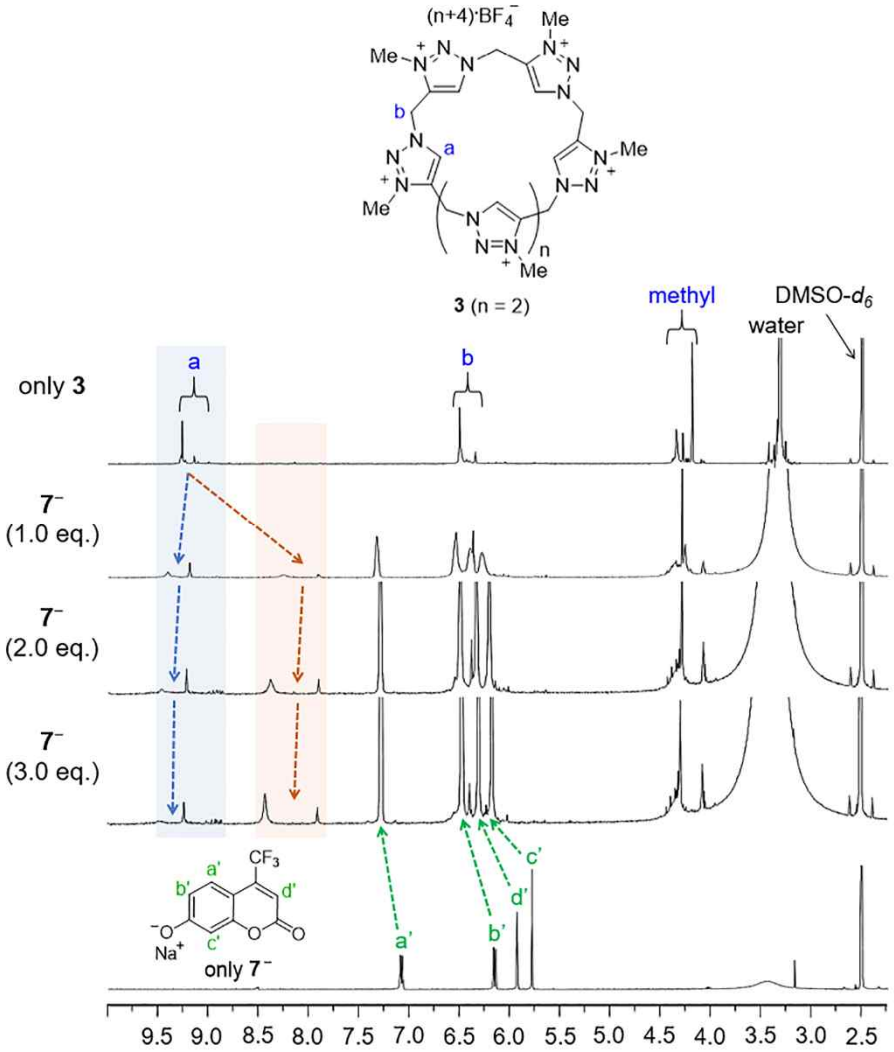

Figure S26. ^{1}H NMR spectra of **3** (2 mM) in DMSO-d_6 recorded in the presence of increasing concentrations of **7**$^{-}$.

6. Indicator displacement for the recognition of AMP

I. Fluorescence spectra of 3/7^{-} complexes in the presence of nucleoside phosphates

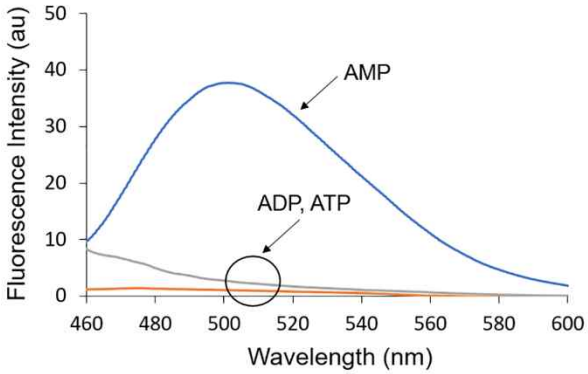

Figure S27. Fluorescence spectra of **3**/**7**$^{-}$ complex (10 μM, λ_{ex} = 410 nm) in the presence of 100 equiv. of adenine nucleotides (as sodium salts, AMP, ADP or ATP) in water.

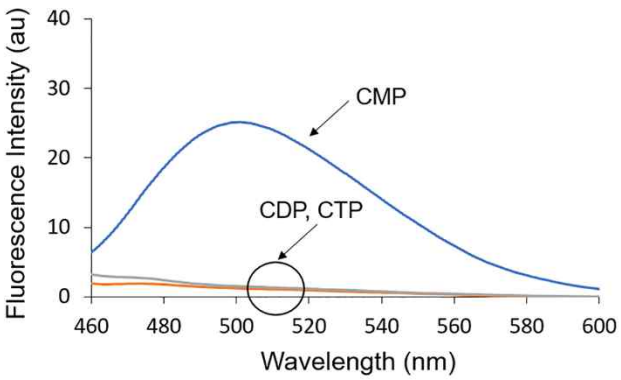

Figure S28. Fluorescence spectra of **3**/**7**$^{-}$ complex (10 μM, λ_{ex} = 410 nm) in the presence of 100 equiv. of cytidine nucleotides (as sodium salts, CMP, CDP or CTP) in water.

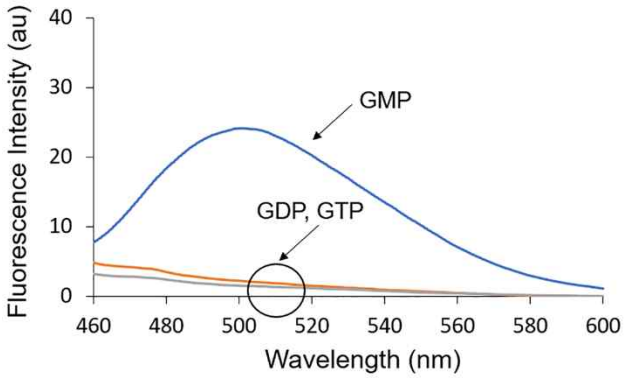

Figure S29. Fluorescence spectra of **3/7**$^{-}$ complex (10 μM, λ_{ex} = 410 nm) in the presence of 100 equiv. of guanosine nucleotides (as sodium salts, GMP, GDP or GTP) in water.

II. Fluorescence spectra of 1–2/7^{-} complexes in the presence of various anions

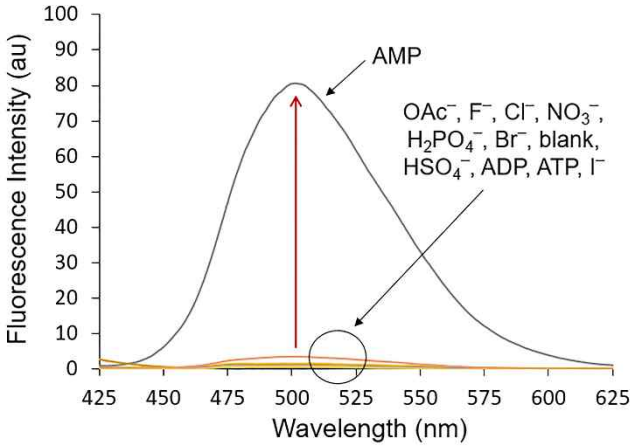

Figure S30. Fluorescence spectra of **1/7**$^{-}$ complex (10 μM, λ_{ex} = 410 nm) in the presence of 100 equiv. of various anions (as sodium salts, F^{-}, Cl^{-}, Br^{-}, I^{-}, $H_2PO_4^{-}$, OAc^{-}, NO_3^{-}, HSO_4^{-}, AMP, ADP or ATP) in water.

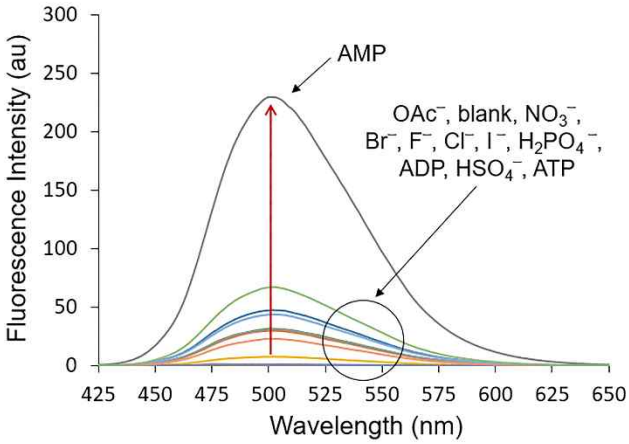

Figure S31. Fluorescence spectra of **2**/**7**$^{-}$ complex (10 μM, λ_{ex} = 410 nm) in the presence of 100 equiv. of various anions (as sodium salts, F^{-}, Cl^{-}, Br^{-}, I^{-}, $H_2PO_4^{-}$, OAc^{-}, NO_3^{-}, HSO_4^{-}, AMP, ADP or ATP) in water.

III. Indicator displacement of 1–3/7^{-} complex with AMP

(1) Fluorescence titration spectra of **1**–**3**/**7**$^{-}$ complex upon addition of AMP

Fluorescence titration of **1**–**3**/**7**$^{-}$ complex with AMP: Stock solutions of calix[n]triazoliums **1**–**3** (50 mM), chromenolate **7**$^{-}$ (10 μM) and AMP (500 mM) in water were prepared separately. An aliquot of 3 mL of **7**$^{-}$ solution was transferred to a cuvette to take an initial spectrum and add the minimum amount of **1**–**3** solution for complete fluorescence quenching of **7**$^{-}$. Aliquots of each AMP solution (0–60 μL) were added to the cuvette and the spectrum was recorded after each addition. The binding constant was analyzed by Bindfit, plotting fluorescence emission values at 500 nm against equivalents of the AMP added. The graph of the indicator displacement of **3**/**7**$^{-}$ complex with AMP is shown in Fig. 4b in the manuscript.

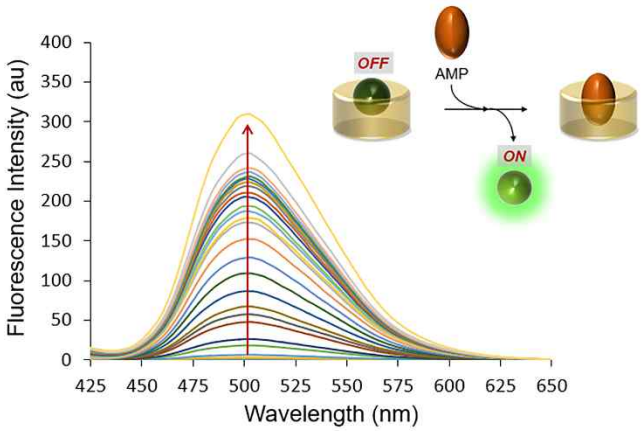

Figure S32. Fluorescence spectra of **1**/**7**$^{-}$ complex (10 μM, λ_{ex} = 410 nm) upon addition of AMP (0–60 μL) in water.

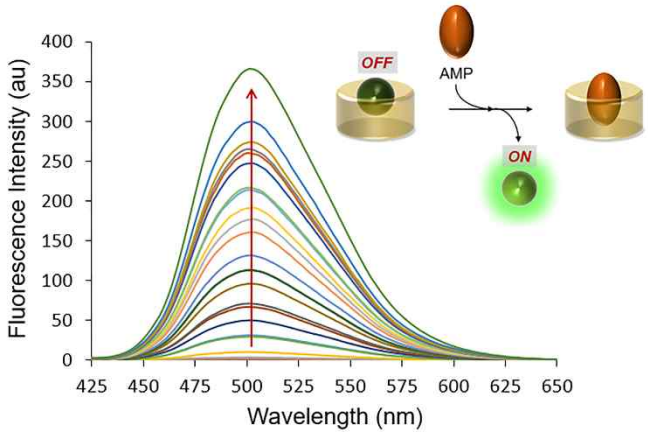

Figure S33. Fluorescence spectra of **2**/**7**$^{-}$ complex (10 μM, λ_{ex} = 410 nm) upon addition of AMP (0–60 μL) in water.

(2) Association constant calculated by bindfit

a. Association constant calculation between **1**/**7**$^{-}$ complex and AMP

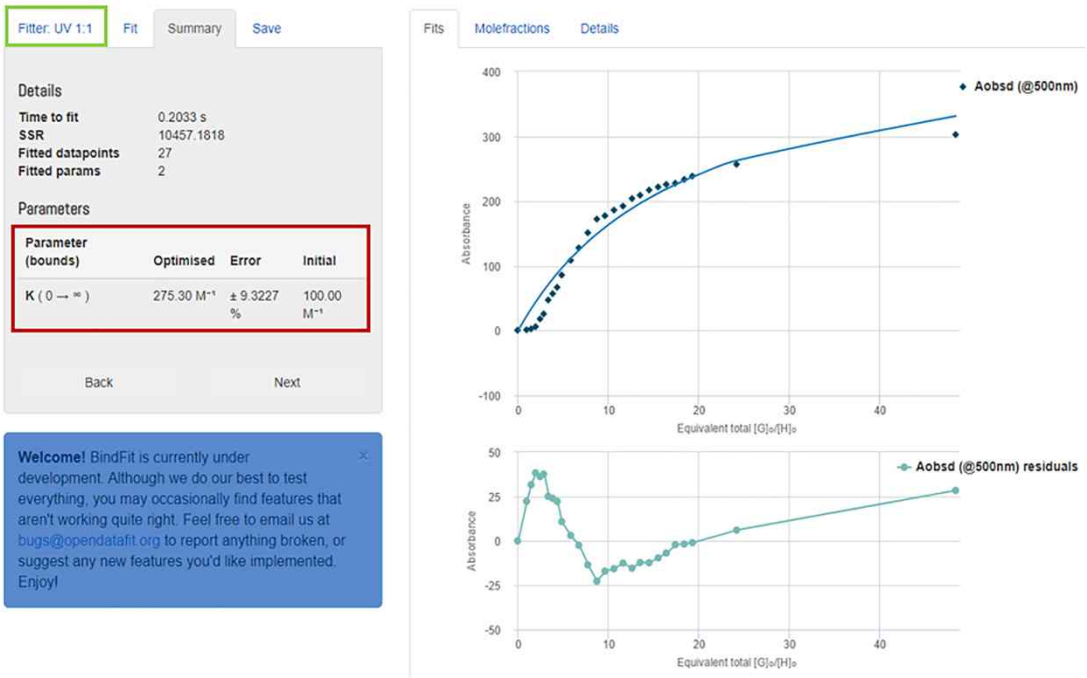

Figure S34. Screenshot of the summary window of http://app.supramolecular.org/bindfit/. This screenshot shows the raw data for fluorescence titration of AMP with **1**/**7**$^{-}$ complex following the fluorescence emission values at 500 nm vs. the data fitted to 1 : 1 UV binding model, the corresponding residual plot and the association constants with the calculated asymptotic standard errors.

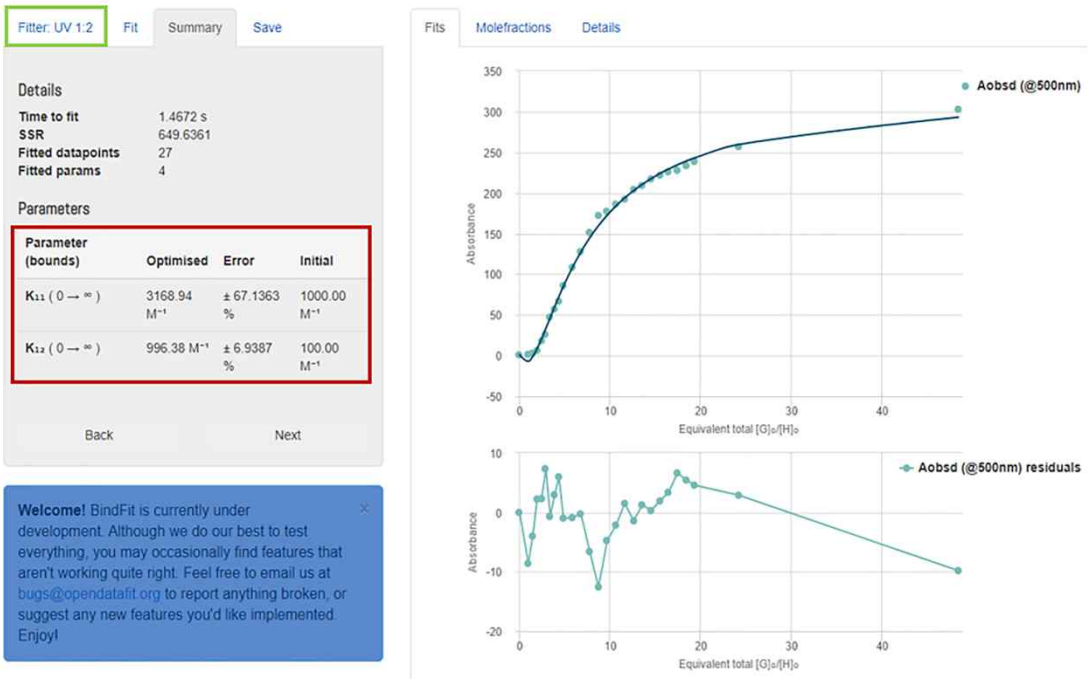

Figure S35. Screenshot of the summary window of http://app.supramolecular.org/bindfit/. This screenshot shows the raw data for fluorescence titration of AMP with **1**/**7**$^{-}$ complex following the fluorescence emission values at 500 nm vs. the data fitted to 1 : 2 UV binding model, the corresponding residual plot and the association constants with the calculated asymptotic standard errors.

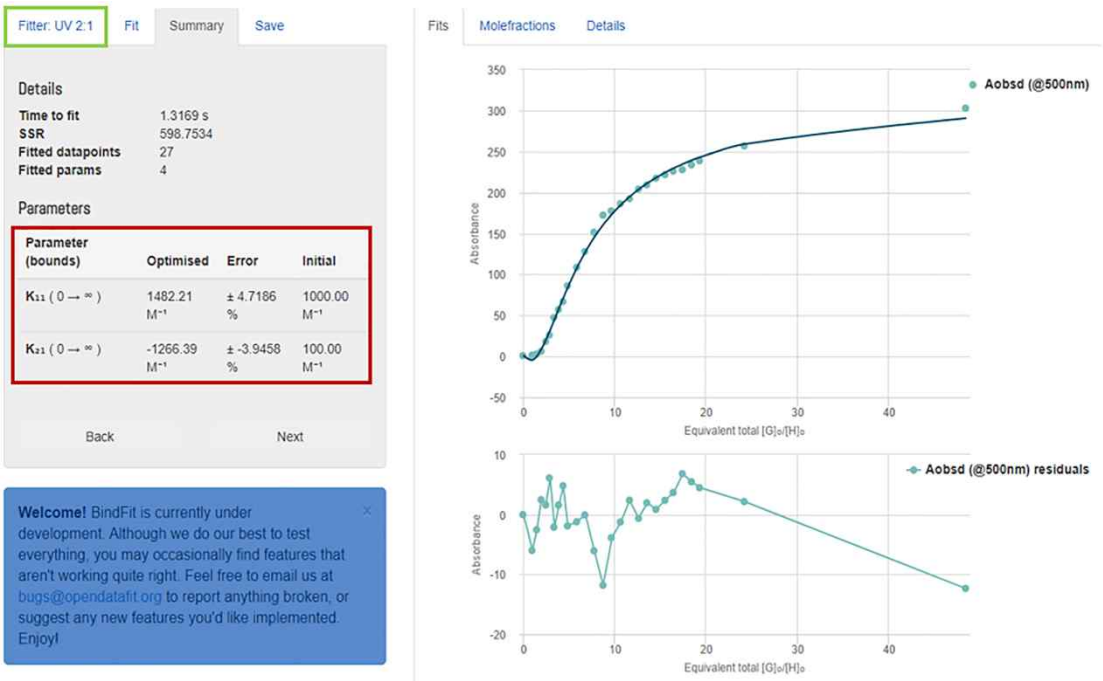

Figure S36. Screenshot of the summary window of http://app.supramolecular.org/bindfit/. This screenshot shows the raw data for fluorescence titration of AMP with **1**/**7**$^{-}$ complex following the fluorescence emission values at 500 nm vs. the data fitted to 2 : 1 UV binding model, the corresponding residual plot and the association constants with the calculated asymptotic standard errors.

Table S8. Summary of association constants between AMP and **1**/**7**$^{-}$ complex according to different binding models.[a]

Binding models		
1 : 1	1 : 2	2 : 1
275.30 (±9.32%)	K_{11} 3168.94 (±67.14%) K_{12} 996.38 (±6.94%)	K_{11} 1482.21 (±4.72%) K_{21} -1266.39 (±-3.95%)

[a] The Bindfit software for data analysis was used from *supramolecular.org*.

b. Association constant calculation between **2**/**7**$^{-}$ complex and AMP

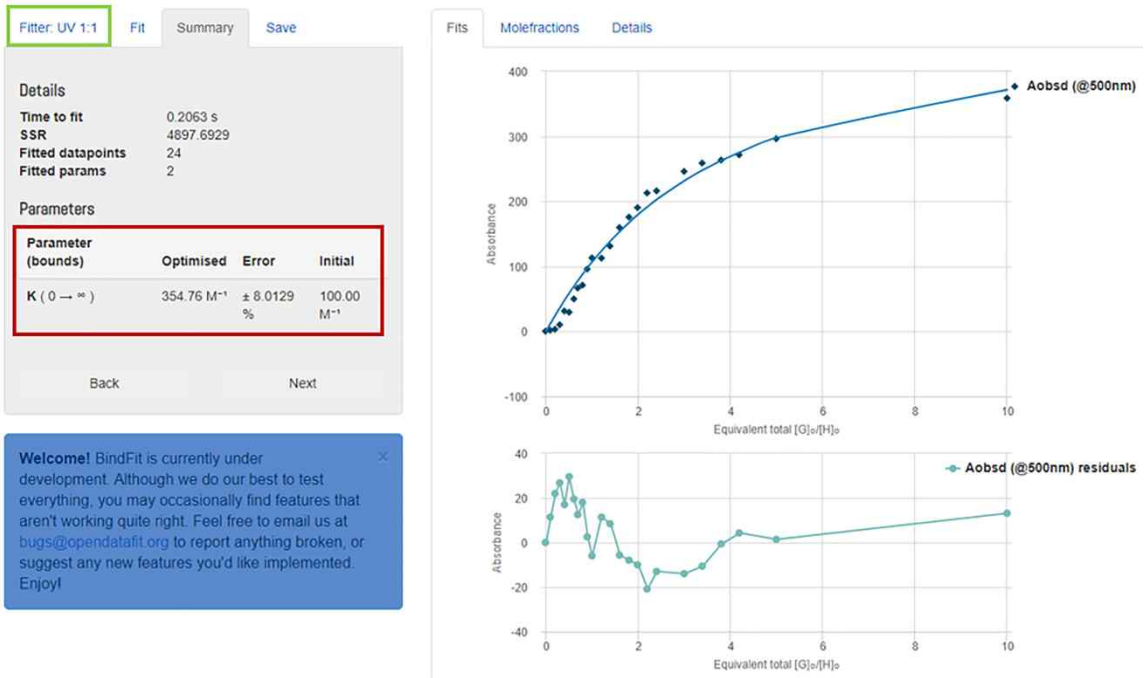

Figure S37. Screenshot of the summary window of http://app.supramolecular.org/bindfit/. This screenshot shows the raw data for fluorescence titration of AMP with **2**/**7**$^{-}$ complex following the fluorescence emission values at 500 nm vs. the data fitted to 1 : 1 UV binding model, the corresponding residual plot and the association constants with the calculated asymptotic standard errors.

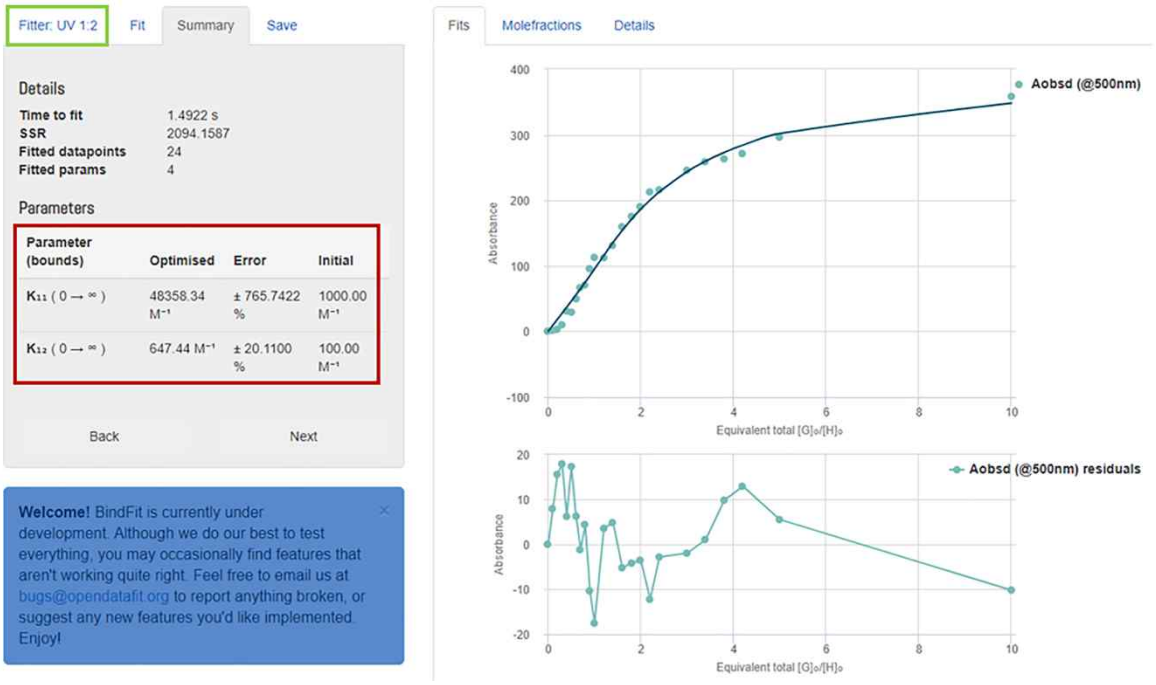

Figure S38. Screenshot of the summary window of http://app.supramolecular.org/bindfit/. This screenshot shows the raw data for fluorescence titration of AMP with **2**/**7**$^{-}$ complex following the fluorescence emission values at 500 nm vs. the data fitted to 1 : 2 UV binding model, the corresponding residual plot and the association constants with the calculated asymptotic standard errors.

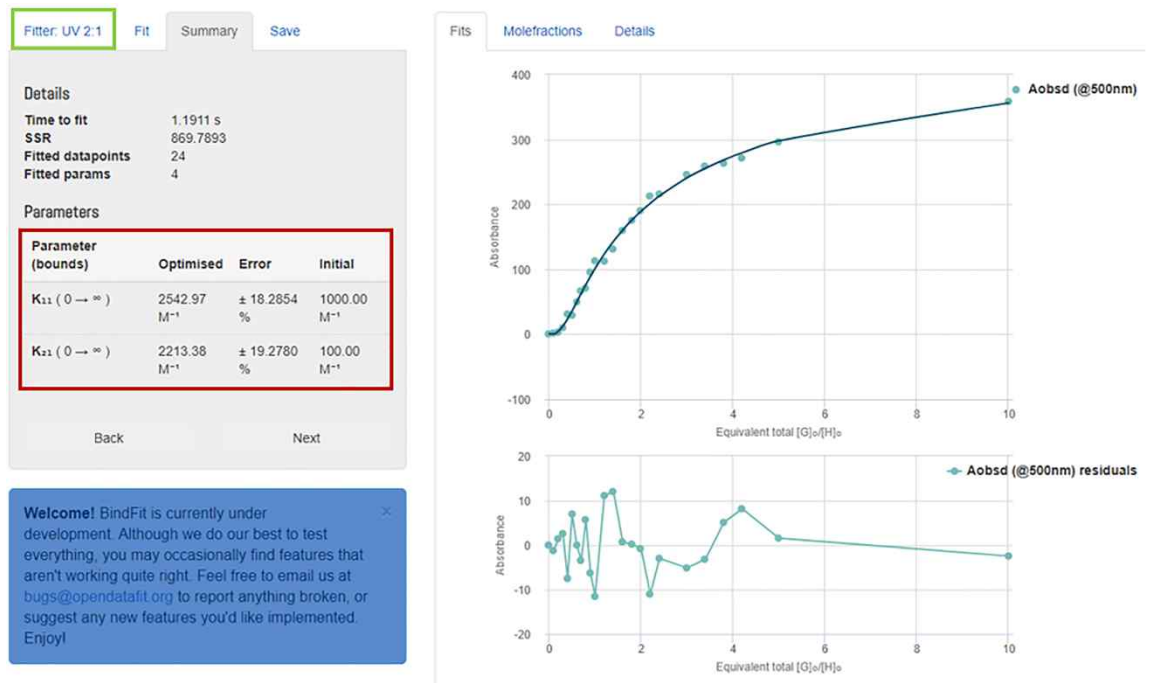

Figure S39. Screenshot of the summary window of http://app.supramolecular.org/bindfit/. This screenshot shows the raw data for fluorescence titration of AMP with **2**/**7**$^{-}$ complex following the fluorescence emission values at 500 nm vs. the data fitted to 2 : 1 UV binding model, the corresponding residual plot and the association constants with the calculated asymptotic standard errors.

Table S9. Summary of association constants between AMP and **2**/**7**$^{-}$ complex according to different binding models.[a]

Binding models		
1 : 1	1 : 2	2 : 1
354.76 (±8.01%)	K_{11} 48358.34 (±765.74%) K_{12} 647.44 (±20.11%)	K_{11} 2542.97 (±18.29%) K_{21} 2213.38 (±19.28%)

[a] The Bindfit software for data analysis was used from *supramolecular.org*.

c. Association constant calculation between **3**/**7**$^{-}$ complex and AMP

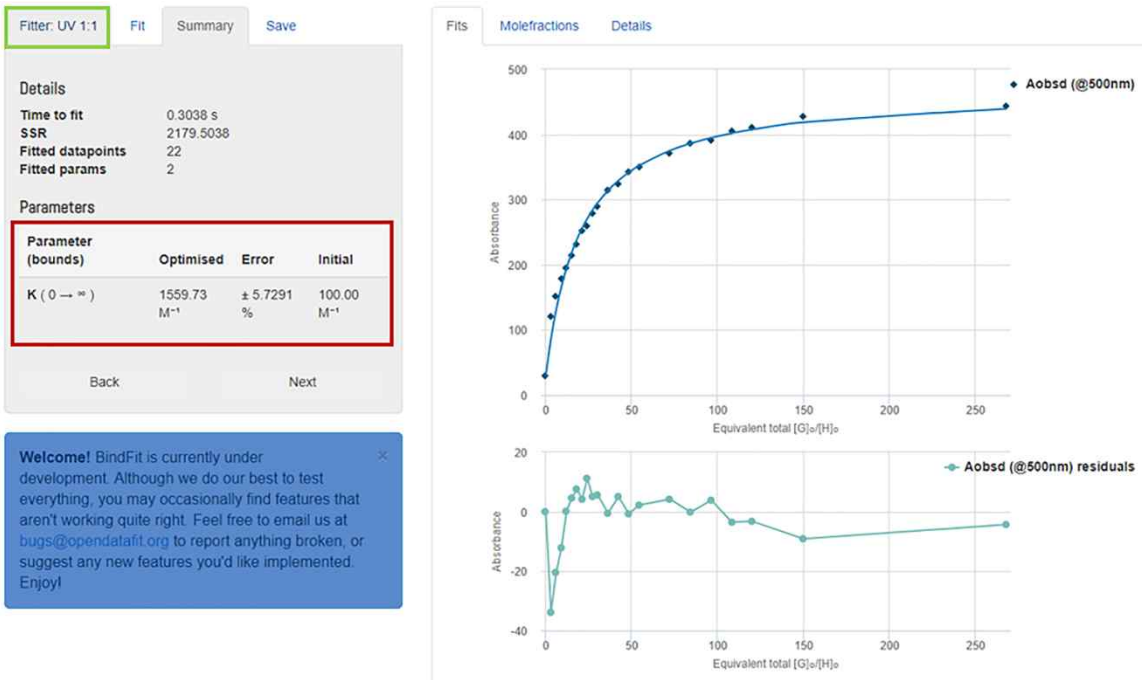

Figure S40. Screenshot of the summary window of http://app.supramolecular.org/bindfit/. This screenshot shows the raw data for fluorescence titration of AMP with **3**/**7**$^{-}$ complex following the fluorescence emission values at 500 nm vs. the data fitted to 1 : 1 UV binding model, the corresponding residual plot and the association constants with the calculated asymptotic standard errors.

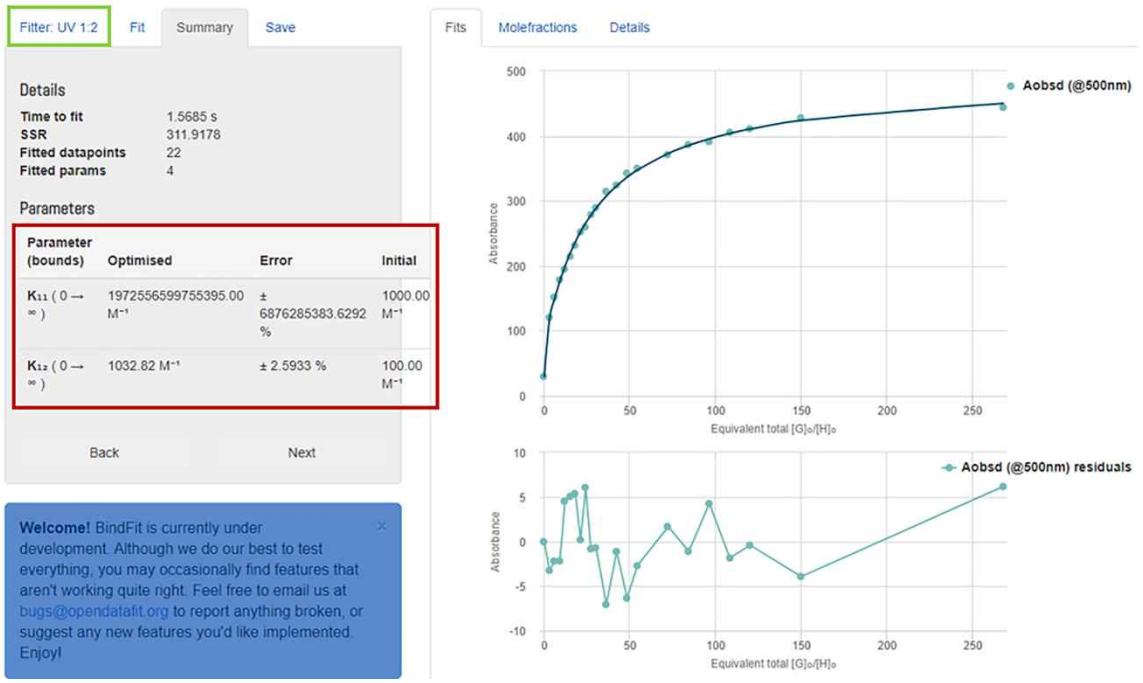

Figure S41. Screenshot of the summary window of http://app.supramolecular.org/bindfit/. This screenshot shows the raw data for fluorescence titration of AMP with **3**/**7**$^{-}$ complex following the fluorescence emission values at 500 nm vs. the data fitted to 1 : 2 UV binding model, the corresponding residual plot and the association constants with the calculated asymptotic standard errors.

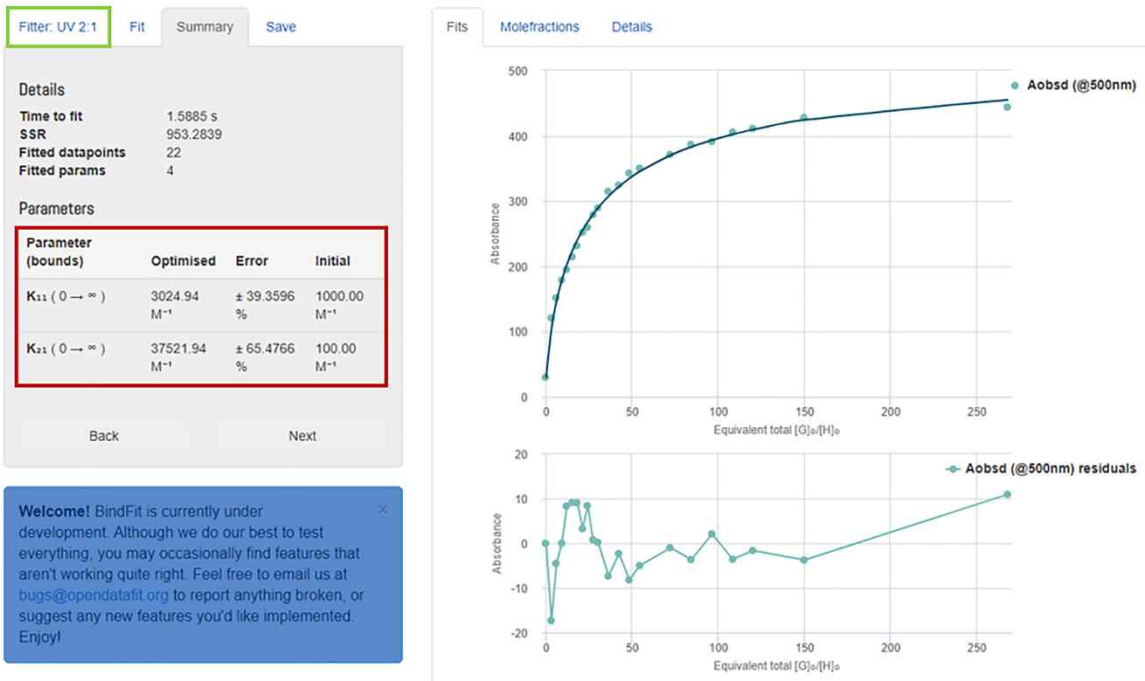

Figure S42. Screenshot of the summary window of http://app.supramolecular.org/bindfit/. This screenshot shows the raw data for fluorescence titration of AMP with **3**/**7**$^{-}$ complex following the fluorescence emission values at 500 nm vs. the data fitted to 2 : 1 UV binding model, the corresponding residual plot and the association constants with the calculated asymptotic standard errors.

Table S10. Summary of association constants between AMP and **3**/**7**$^{-}$ complex according to different binding models.[a]

Binding models		
1 : 1	1 : 2	2 : 1
1559.73 (±5.73%)	K_{11} 1972556599755395.00 (± 6876285383.63%) K_{12} 1032.82 (±2.59%)	K_{11} 3024.94 (±39.36%) K_{21} 37521.94 (±65.48%)

[a] The Bindfit software for data analysis was used from *supramolecular.org*.

(3) ^{1}H NMR titration spectra of **3** upon addition of AMP to calculate the association constant

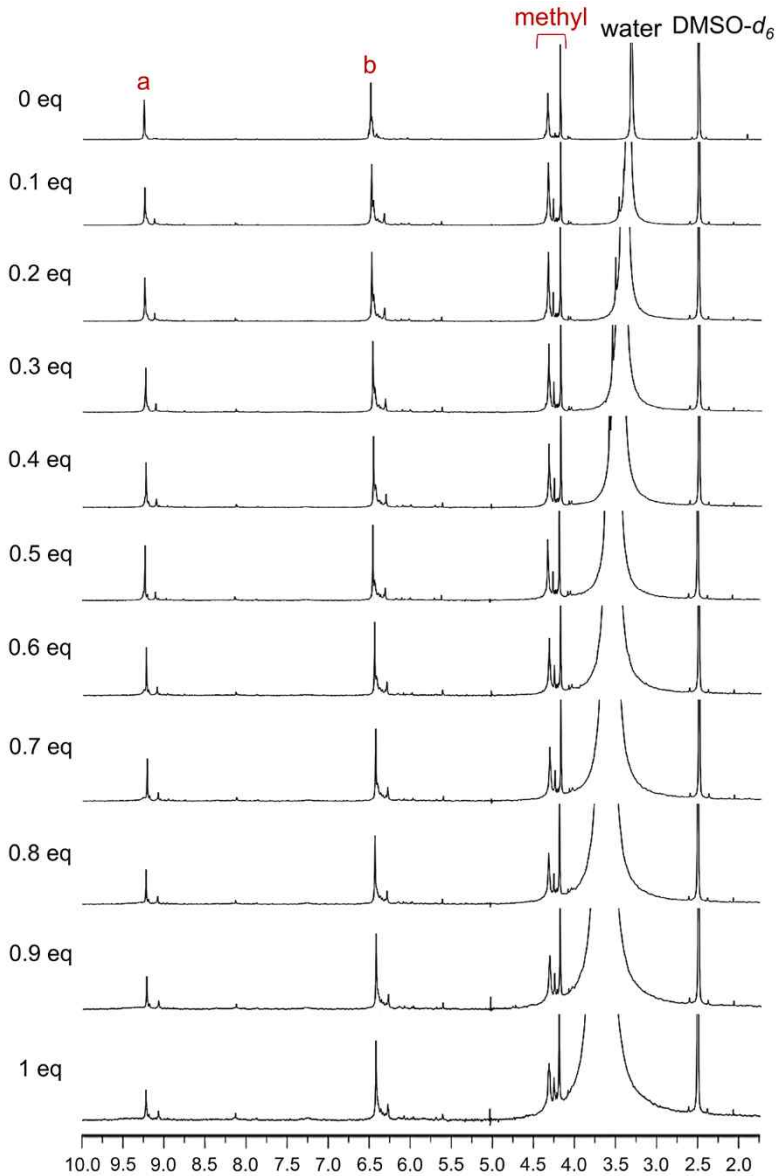

Figure S43. ^{1}H NMR titration spectra of **3** (4 mM) upon addition of AMP (0–1 equiv.) in DMSO-d_6.

(4) Association constant between **3** and AMP calculated by bindfit

Figure S44. Screenshot of the summary window of http://app.supramolecular.org/bindfit/. This screenshot shows the raw data for ^{1}H NMR titration of **3** with AMP following the triazolium C5–H signal vs. the data fitted to 1 : 1 NMR binding model, the corresponding residual plot and the association constants with the calculated asymptotic standard errors.

Figure S45. Screenshot of the summary window of http://app.supramolecular.org/bindfit/. This screenshot shows the raw data for ^{1}H NMR titration of **3** with AMP following the triazolium C5–H signal vs. the data fitted to 1 : 2 NMR binding model, the corresponding residual plot and the association constants with the calculated asymptotic standard errors.

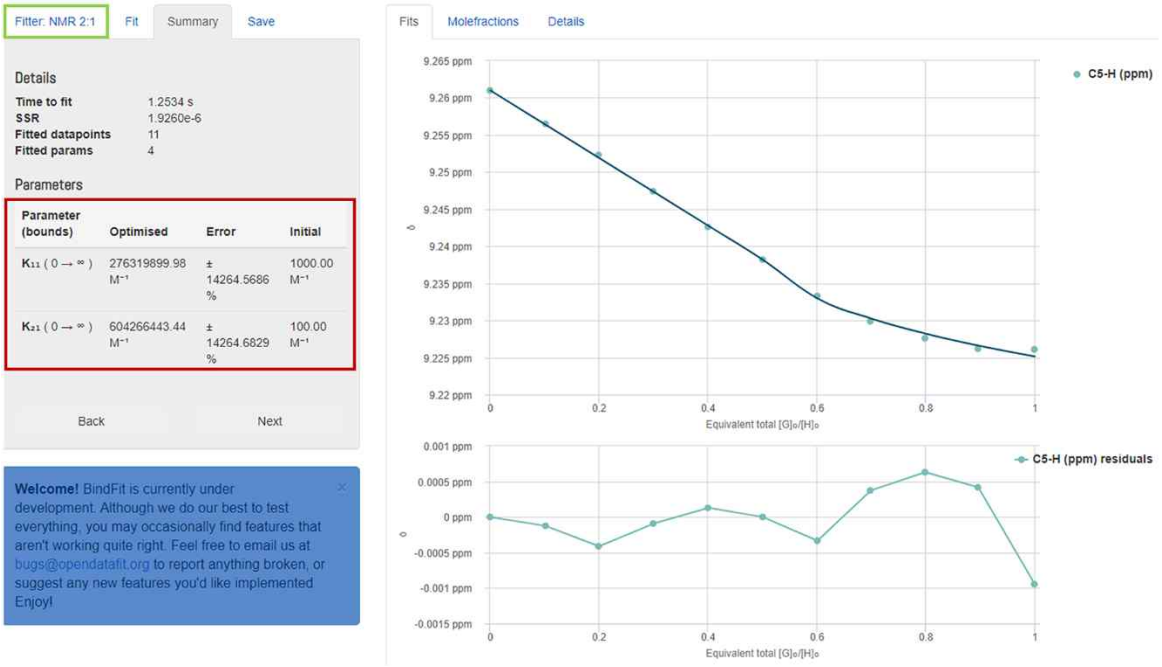

Figure S46. Screenshot of the summary window of http://app.supramolecular.org/bindfit/. This screenshot shows the raw data for ^{1}H NMR titration of **3** with AMP following the triazolium C5–H signal vs. the data fitted to 2 : 1 NMR binding model, the corresponding residual plot and the association constants with the calculated asymptotic standard errors.

Table S11. Summary of association constants between AMP and **3** according to different binding models.[a]

Binding models		
1 : 1	1 : 2	2 : 1
3517.59 (±20.31%)	K_{11} 37964.66 (±48.88%) K_{12} 20.23 (±47.19%)	K_{11} 276319899.98 (±14264.57%) K_{21} 604266443.44 (±14264.68%)

[a] The Bindfit software for data analysis was used from *supramolecular.org*.

(5) ^{1}H NMR spectra of **4** and **1**–**3** in the presence of increasing concentrations of AMP

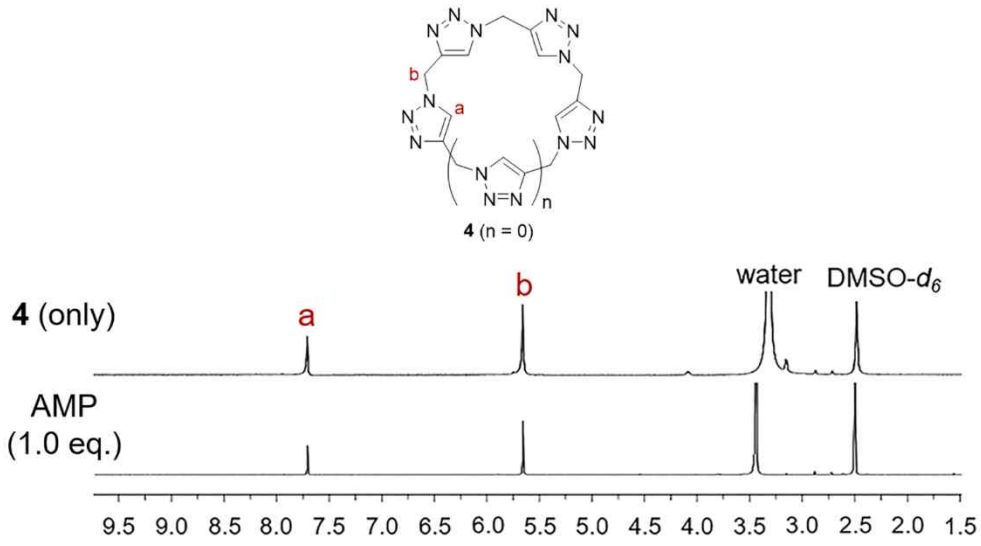

Figure S47. ^{1}H NMR spectra of **4** (2mM) in DMSO-d_6 recorded in the presence of AMP (1 equiv.).

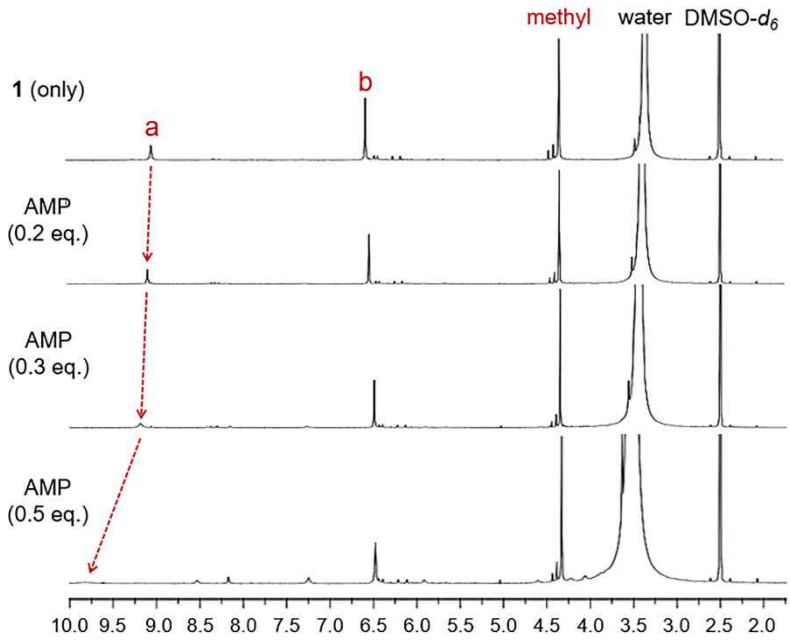

Figure S48. ^{1}H NMR spectra of **1** (2mM) in DMSO-d_6 recorded in the presence of increasing concentrations of AMP.

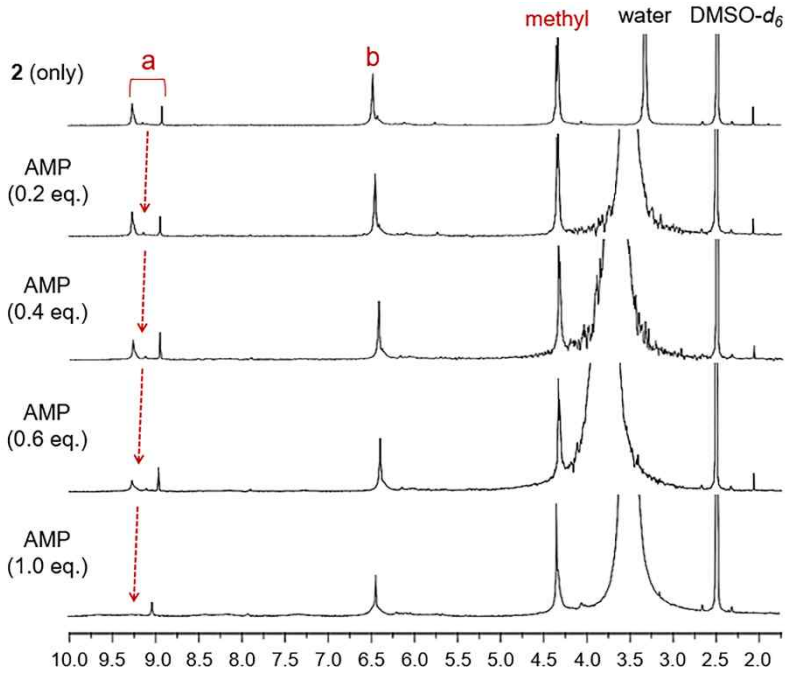

Figure S49. ^{1}H NMR spectra of **2** (2mM) in DMSO-d_6 recorded in the presence of increasing concentrations of AMP.

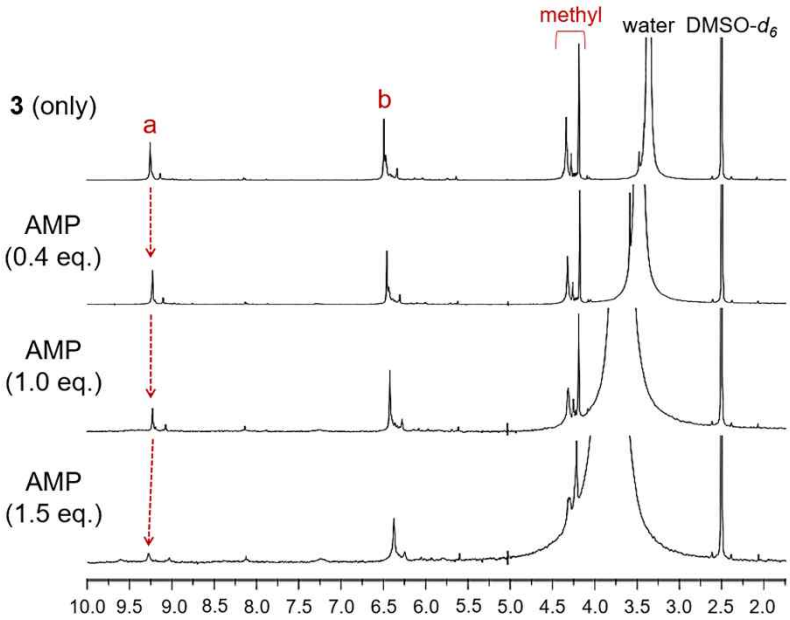

Figure S50. ^{1}H NMR spectra of **3** (2mM) in DMSO-d_6 recorded in the presence of increasing concentrations of AMP.

(6) ^{1}H NMR spectra of AMP in the presence of increasing concentrations of **1**–**3**

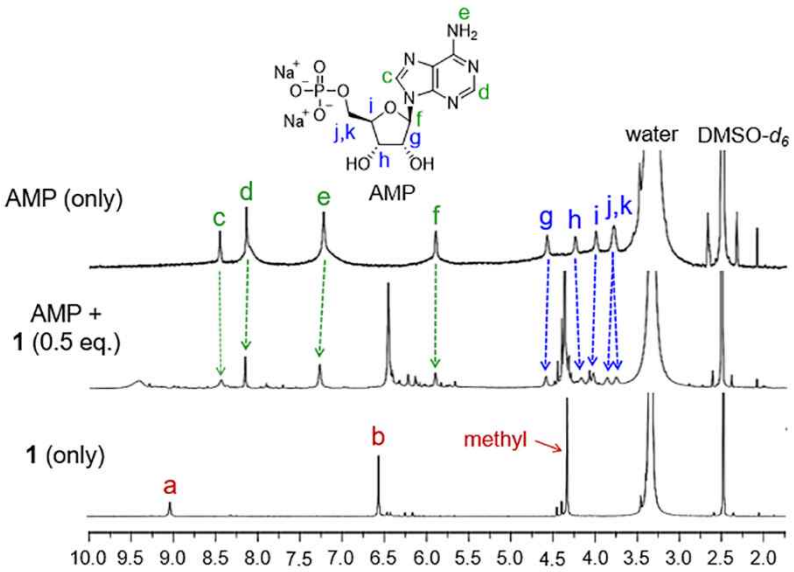

Figure S51. ^{1}H NMR spectra of AMP (4 mM) in DMSO-d_6 recorded in the presence of increasing concentrations of **1**.

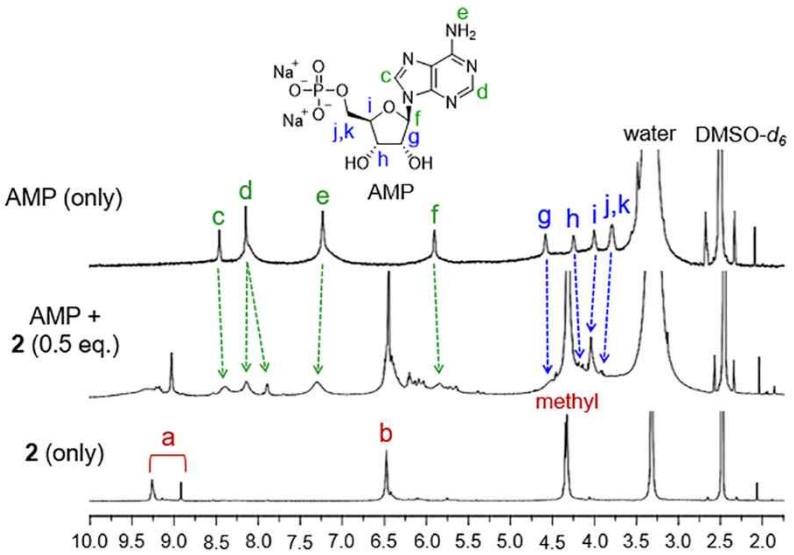

Figure S52. ^{1}H NMR spectra of AMP (4 mM) in DMSO-d_6 recorded in the presence of increasing concentrations of **2**.

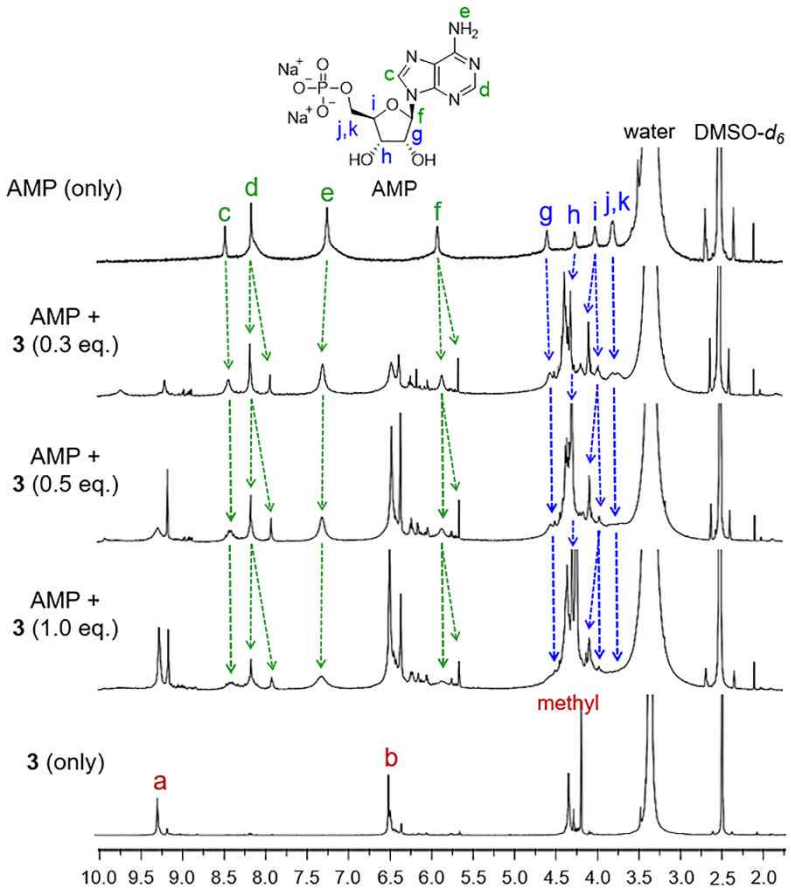

Figure S53. ^{1}H NMR spectra of AMP (4 mM) in DMSO-d_6 recorded in the presence of increasing concentrations of **3**.

(7) ^{31}P NMR spectra of AMP with calix[n]triazoliums (**1**–**3**)

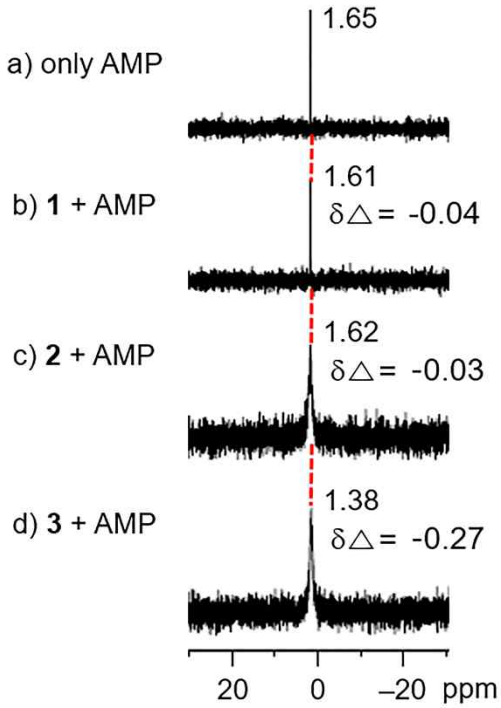

Figure S54. ^{31}P NMR spectra of (a) AMP (2 mM) and (b) with 0.1 equiv. of **1** (c) with 0.1 equiv. of **2** (d) with 0.1 equiv. of **3** in D_2O.

7. References

S1 I. Kim, K. C. Ko, W. R. Lee, J. Cho, J. H. Moon, D. Moon, A. Sharma, J. Y. Lee, J. S. Kim and S. Kim, *Org. Lett.*, 2017, **19**, 5509–5512.

S2 J. W. Shin, K. Eom and D. Moon, *J. Synchrotron Radiat.*, 2016, **23**, 369–373.

S3 (a) Z. Otwinowski and W. Minor, in *Methods of Enzymology, Macromolecular Crystallography*, part. A, eds. C. W. Carter and R. M. Sweet, Academic Press, New York, 1997, vol. 276, pp. 307–326. (b) Z. Otwinowski, D. Borek, W. Majewski and W. Minor, *Acta Crystallogr., Sect. A: Found. Crystallogr.*, 2003, **59**, 228–234.

S4 (a) T. Clark, J. Chandrasekhar, G. W. Spitznagel and P. v. R. Schleyer, *J. Comput. Phys.*, 1983, **4**, 294–301. (b) M. J. Frisch, J. A. Pople and J. S. Binkley, *J. Chem. Phys.*, 1984, **80**, 3265–3269. (c) J.-D. Chai and M. Head-Gordon, *Phys. Chem. Chem. Phys.*, 2008, **10**, 6615–6620.

S5 Gaussian 16, Revision A.03, M. J. Frisch, G. W. Trucks, H. B. Schlegel, G. E. Scuseria, M. A. Robb, J. R. Cheeseman, G. Scalmani, V. Barone, G. A. Petersson, H. Nakatsuji, X. Li, M. Caricato, A. V. Marenich, J. Bloino, B. G. Janesko, R. Gomperts, B. Mennucci, H. P. Hratchian, J. V. Ortiz, A. F. Izmaylov, J. L. Sonnenberg, D. Williams-Young, F. Ding, F. Lipparini, F. Egidi, J. Goings, B. Peng, A. Petrone, T. Henderson, D. Ranasinghe, V. G. Zakrzewski, J. Gao, N. Rega, G. Zheng, W. Liang, M. Hada, M. Ehara, K. Toyota, R. Fukuda, J. Hasegawa, M. Ishida, T. Nakajima, Y. Honda, O. Kitao, H. Nakai, T. Vreven, K. Throssell, J. A. Montgomery, Jr., J. E. Peralta, F. Ogliaro, M. J. Bearpark, J. J. Heyd, E. N. Brothers, K. N. Kudin, V. N. Staroverov, T. A. Keith, R. Kobayashi, J. Normand, K. Raghavachari, A. P. Rendell, J. C. Burant, S. S. Iyengar, J. Tomasi, M. Cossi, J. M. Millam, M. Klene, C. Adamo, R. Cammi, J. W. Ochterski, R. L. Martin, K. Morokuma, O. Farkas, J. B. Foresman and D. J. Fox, Gaussian, Inc., Wallingford CT, 2016.

S6 A. R. Allouche, *J. Comput. Chem.*, 2011, **32**, 174–182.

8. NMR Spectra

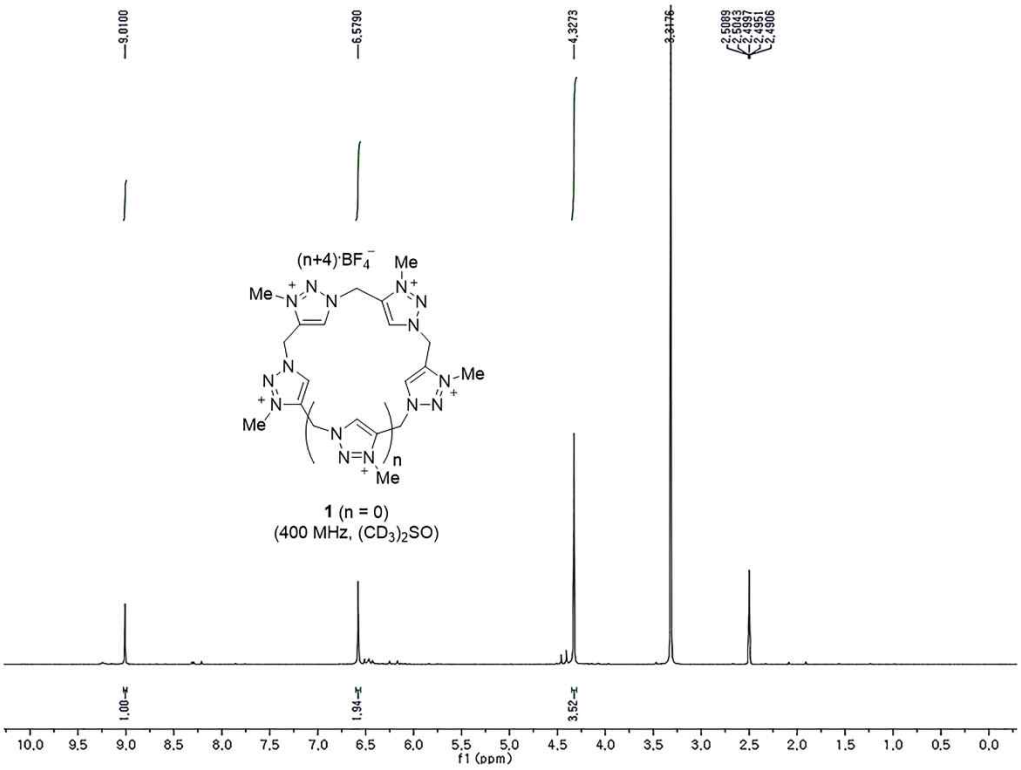

^{1}H NMR spectrum of compound **1**.

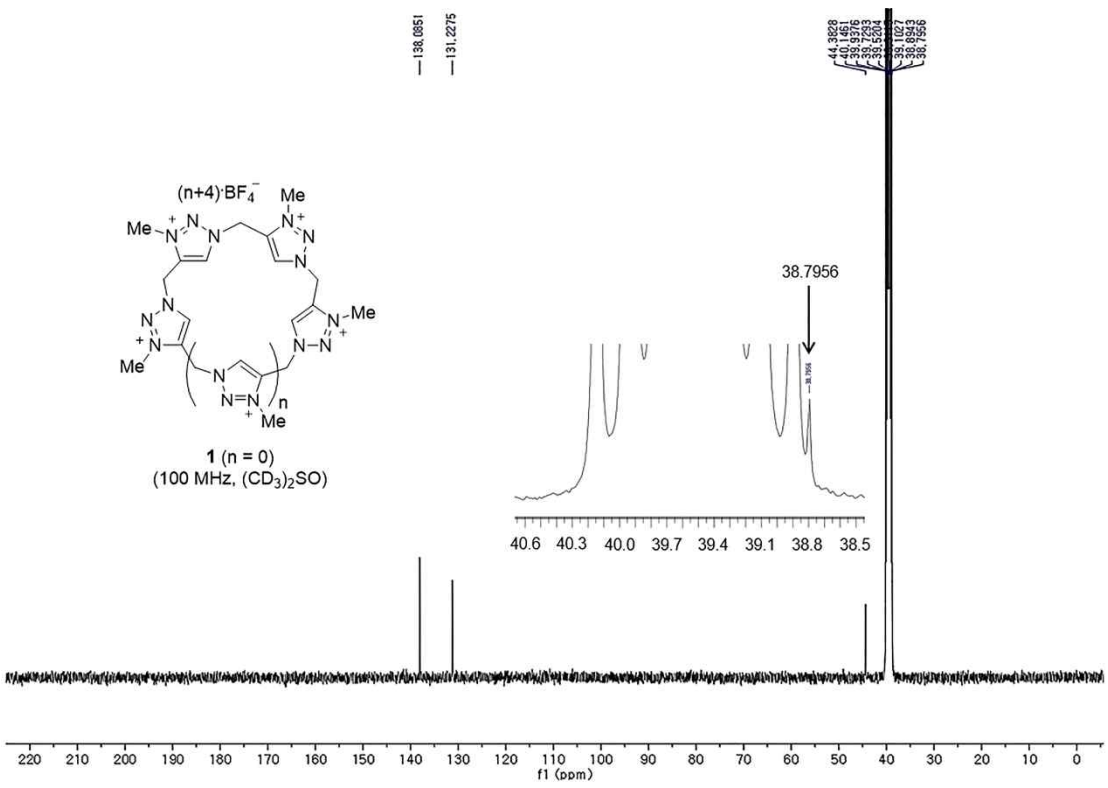

^{13}C NMR spectrum of compound **1**.

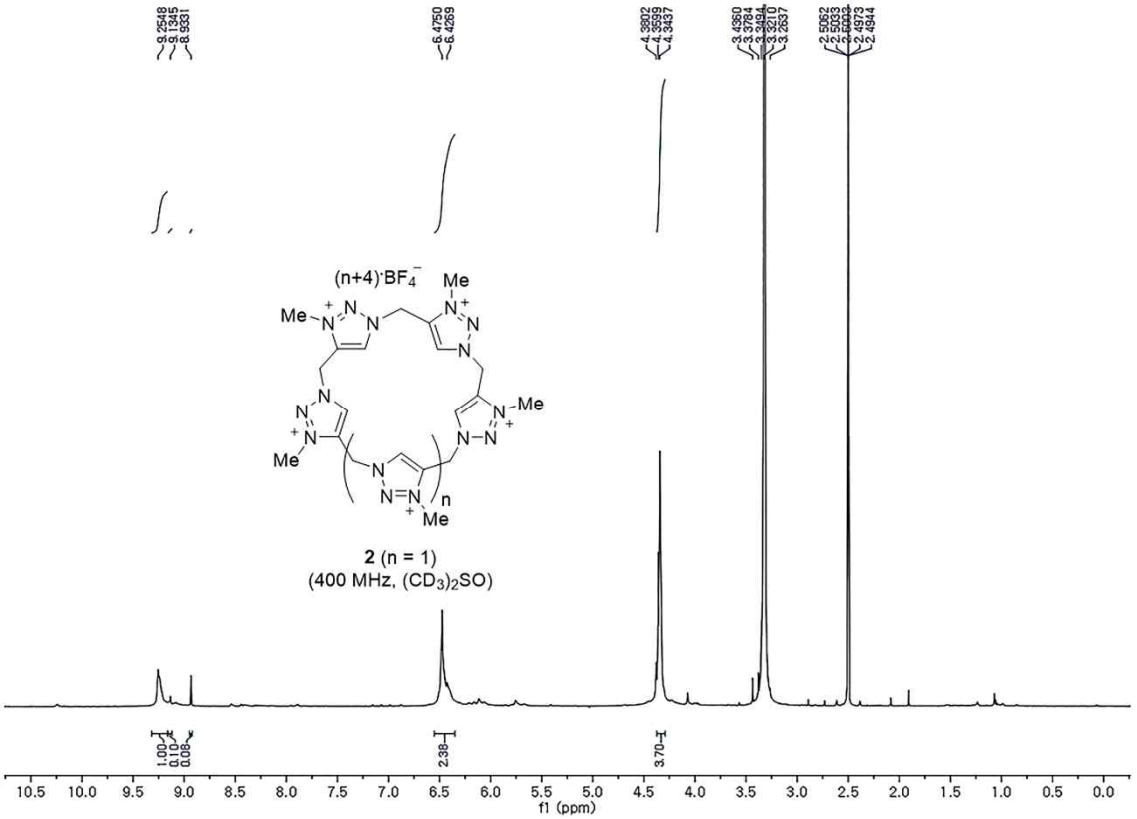

^{1}H NMR spectrum of compound **2**.

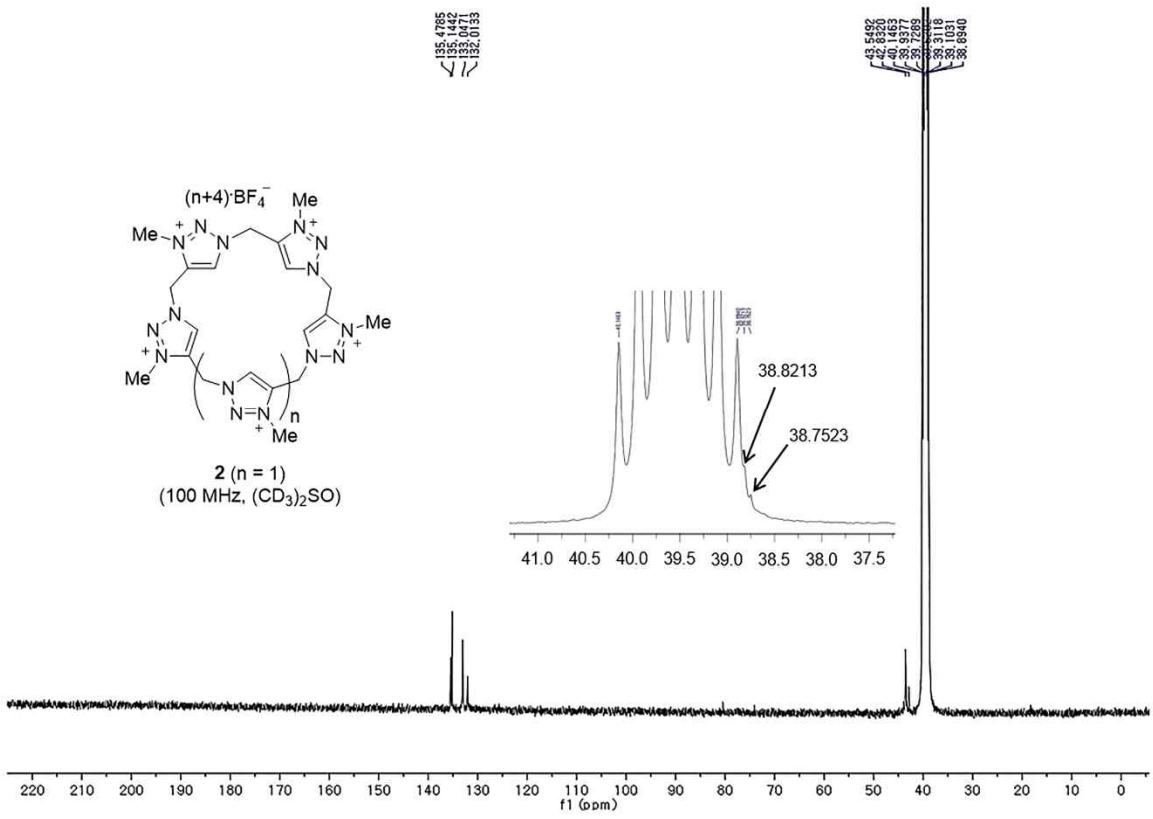

^{13}C NMR spectrum of compound **2**.

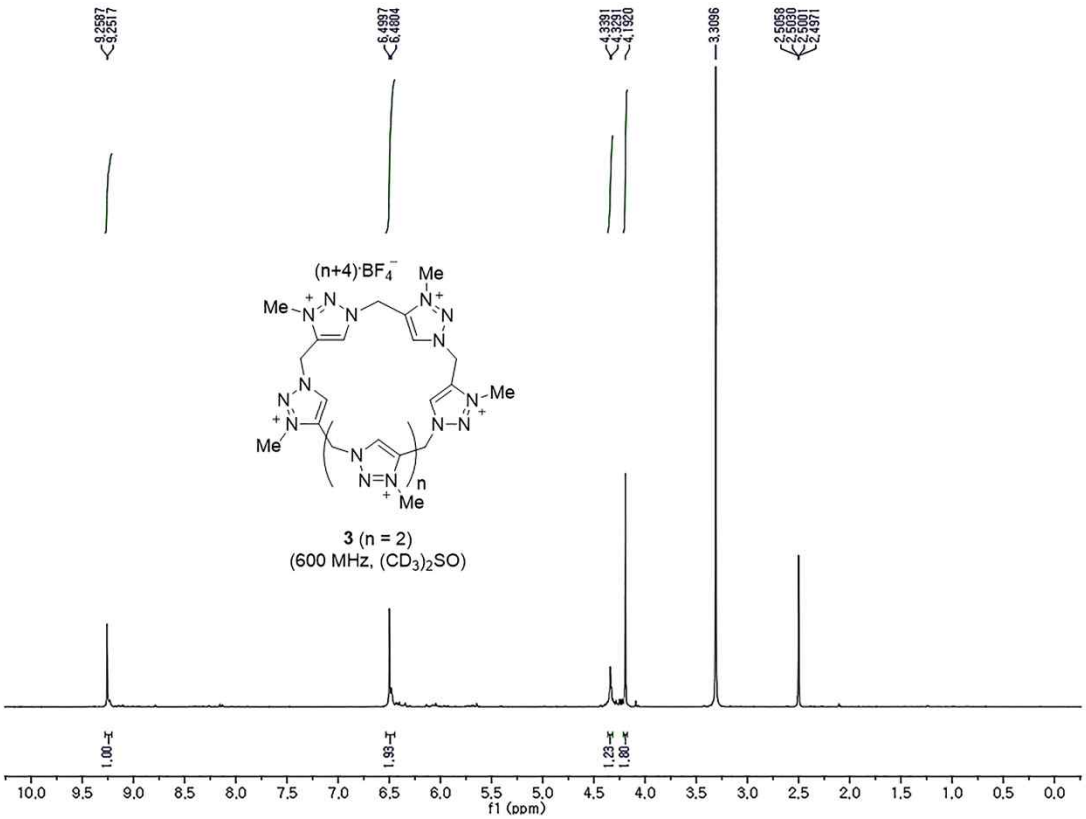

^{1}H NMR spectrum of compound **3**.

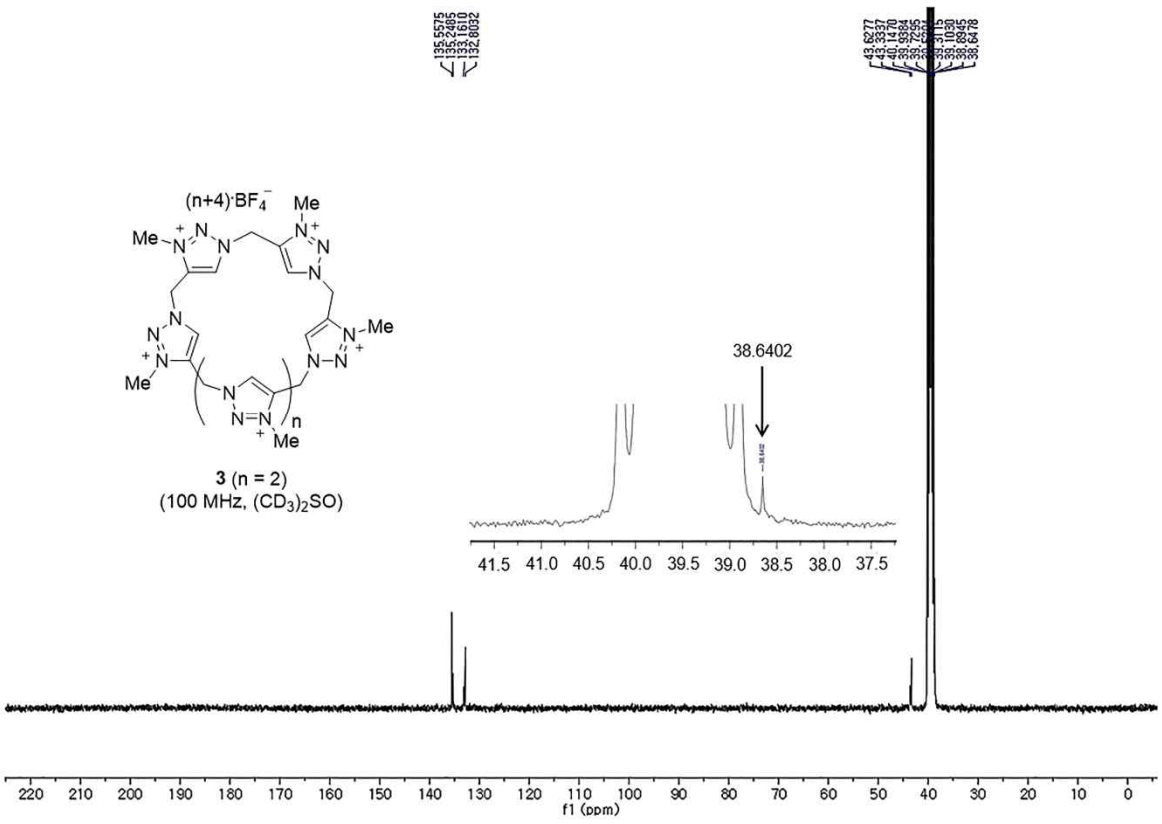

^{13}C NMR spectrum of compound **3**.

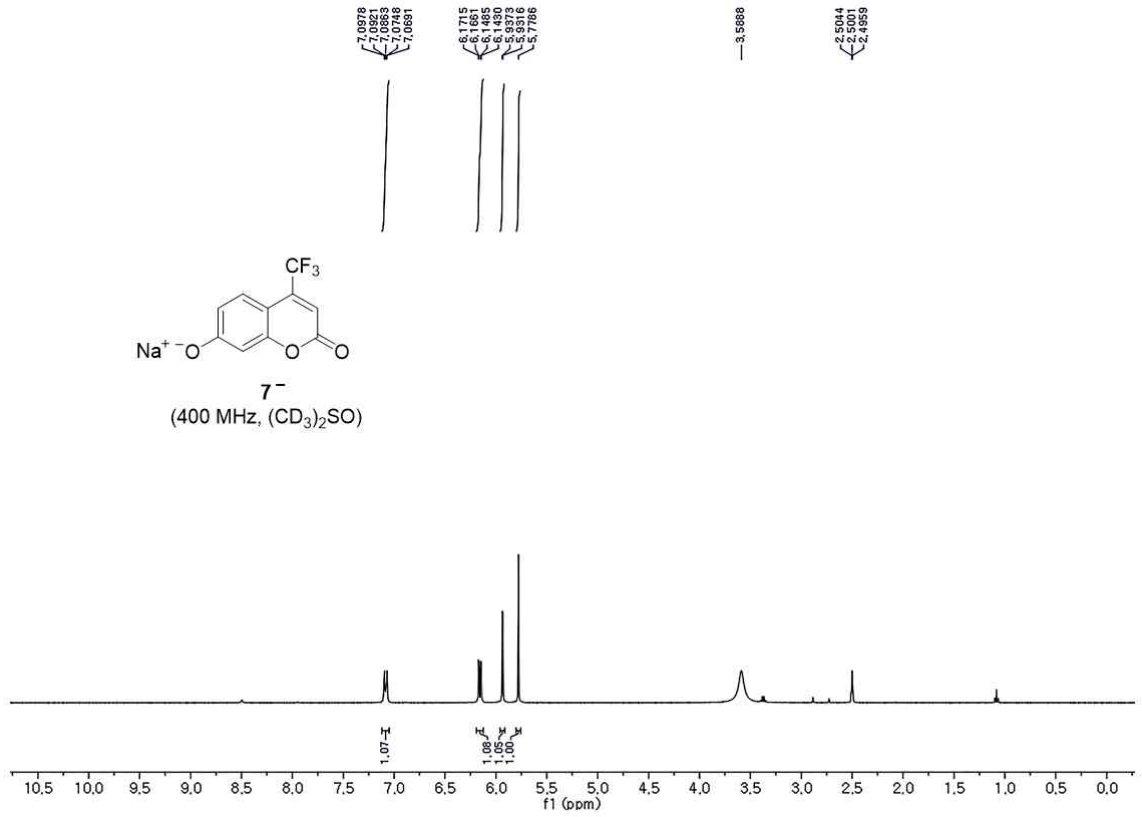

^{1}H NMR spectrum of compound **7**$^{-}$.

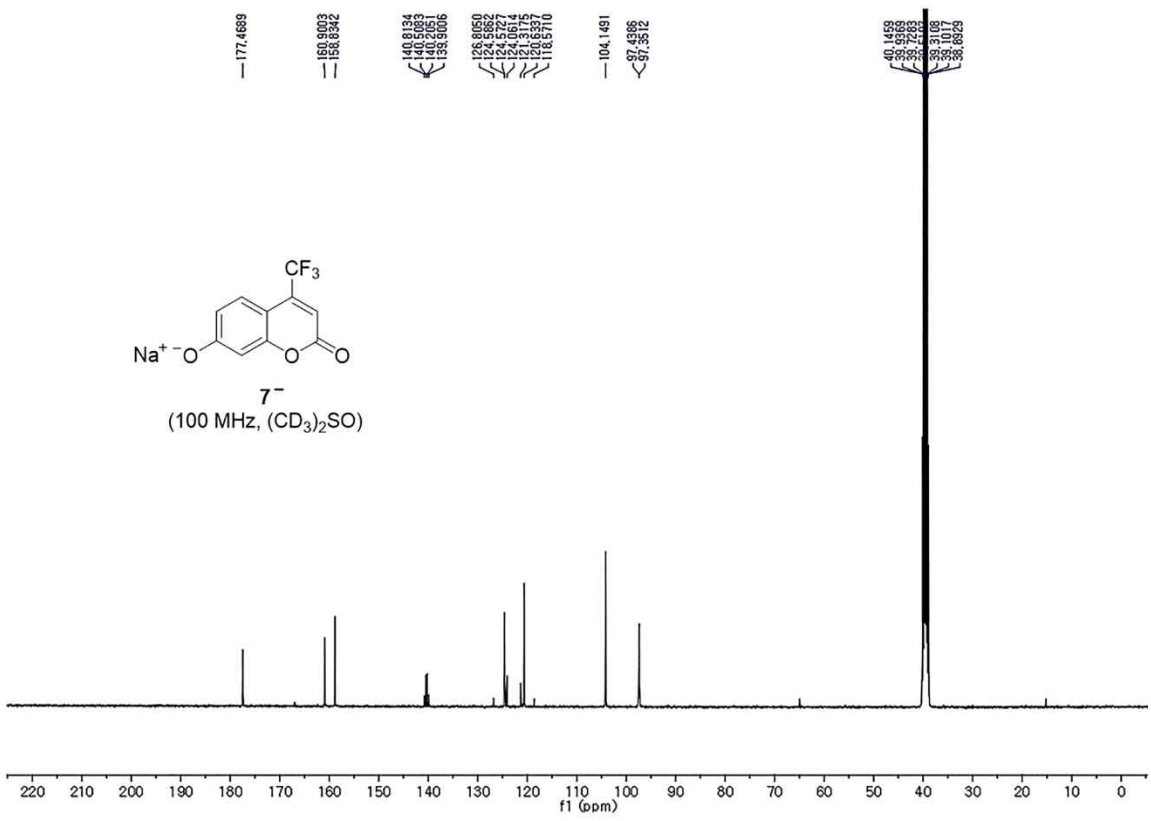

^{13}C NMR spectrum of compound **7**$^{-}$.